https://doi.org/10.5194/egusphere-2026-2688
Preprint. Discussion started: 11 June 2026

A Triple-Structured Mesospheric Climate Pattern Driven by a Double-Celled Meridional Circulation during the Equinox-Solstice Transition Months of November and May

Liang Zhang[1], Zhongfang Liu[1]

[1]State Key Laboratory of Marine Geology, Tongji University, Shanghai, 200092, China

Correspondence to: Liang Zhang (Liangzhang420@tongji.edu.cn)

Abstract. The upper mesosphere is a dynamically and chemically complex region where interannual climate variability remains incompletely understood, particularly during the transition months between the equinox and solstice circulation regimes. Using multi-satellite observations from MLS and SABER, we investigate the coupled dynamical-microphysical-chemical-thermal structures during November and May, building on the bottom-up mechanism of "upwelling—water vapor (H_2O)—ozone (O_3)—temperature". We employ temperature near 80 km (the T80 index) as a proxy for upwelling intensity and identify two distinct centers: a summer polar upwelling and a tropical upwelling. Together they drive a double-celled anomalous meridional circulation that organizes the global climate into a novel triple-structured pattern, with coherent signatures in the summer high-latitude, equatorial, and winter high-latitude regions. A key finding is that hydration occurs below polar mesospheric clouds (PMCs) without pronounced dehydration above them. This "hydration-without-dehydration" configuration, made possible by the weak PMCs typical of November and May, indicates the dominance of the cold-trap effect over the conventional freeze-drying effect. The absence of dehydration further isolates the temperature-dependent ozone kinetic pathway for polar ozone enhancement, a pathway that is otherwise convolved with dehydration effects in stronger PMC seasons. Ozone and atomic oxygen (O) respond to the combined influences of meridional H_2O transport and local thermal forcing, and the resulting radiative and chemical heating governs temperatures near 90 km (T90). These results establish the structure of the transitional climate regime, demonstrating that the shift from symmetric (equinox) to antisymmetric (solstice) variability is mediated by a well-organized, upwelling-driven double-celled circulation.

1 Introduction

1.1 Mesospheric dynamics

The mesosphere and lower thermosphere (MLT) is the transition region between Earth's atmosphere and space, hosting phenomena such as polar mesospheric clouds (PMCs), polar mesospheric summer echoes (PMSEs), the secondary ozone layer (at ~92 km), metal layers, and airglows (*Plane et al.*, 2023). The summer polar mesopause is the coldest region in

https://doi.org/10.5194/egusphere-2026-2688
Preprint. Discussion started: 11 June 2026

Earth's atmosphere, with temperatures as low as 130 K due to the adiabatic cooling of gravity wave-driven upwelling (*Garcia and Solomon*, 1985; *Holton*, 1983; *Lindzen*, 1981). During solstice months, zonal winds are westward below ~90 km and eastward above, and the residual meridional circulation flows from the summer pole towards the winter pole (*Becker*, 2012; *Ramesh et al.*, 2024). Observations have suggested the possibility of multi-celled meridional circulations in the upper mesosphere, deviating from the conventional single-celled summer-to-winter pattern (*Balsley and Riddle*, 1984; *Eswaraiah et al.*, 2011).

Despite the central importance of vertical winds in controlling the transport of momentum, energy, and chemical constituents in the MLT, direct measurements remain challenging: vertical winds are only a few cm s^{-1} in general circulation models (*Smith*, 2012), beyond the routine observing capabilities of most instruments. While recent advances in multistatic meteor radar (*Stober et al.*, 2022; *Urco et al.*, 2024; *Zeng et al.*, 2024), PMSE radar (*Gudadze et al.*, 2019), and metal lidar (*Yuan et al.*, 2014) have improved our observing capabilities, continuous long-term vertical wind datasets remain unavailable.

To circumvent this limitation, the zonal- and monthly-mean temperatures near 80 km have recently been proposed as a proxy for mesospheric upwelling intensity (*Zhang et al.*, 2025b; *Zhang et al.*, 2025c). This proxy exploits the fact that temperatures at this altitude are dominated by adiabatic processes, with negligible radiative and chemical heating owing to the extremely low ozone concentrations. *Zhang et al.* (2025c) identified solstice anomalous meridional circulations driven by summer polar upwellings, and *Zhang et al.* (2025b) identified equinox anomalous meridional circulations driven by tropical upwellings. November and May are the transition months between these two regimes, during which mesospheric dynamics are potentially governed by both polar and tropical upwellings. This paper aims to unravel the circulation structure during these months and its implications for mesospheric chemistry and climate.

1.2 PMCs and mesospheric H_2O

PMCs form in the summer high-latitude mesosphere between 80 km and 90 km and have long been regarded as potential indicators of climate changes (*Rapp and Thomas*, 2006). Their formation is conventionally described by the growth-sedimentation (GS) scheme, in which nucleation occurs at the cloud top, followed by particle growth and gravitational sedimentation, with sublimation occurring below the saturated zone (*Hultgren and Gumbel*, 2014). This top-down process produces dehydration above PMCs and hydration below, termed the freeze-drying effect (*Berger and von Zahn*, 2002; *Hervig et al.*, 2003; *Summers et al.*, 2001; *von Zahn and Berger*, 2003). In this framework, hydration below PMCs is causally dependent on dehydration above.

As an alternative to the GS scheme, the charged meteoric smoke particle nucleation (CMN) scheme has been proposed for understanding PMC microphysics on zonal and daily scales (*Zhang et al.*, 2025a). The CMN scheme is based on two postulates: charged meteoric smoke particles act as ice nuclei (*Guiu et al.*, 2025; *Gumbel and Megner*, 2009; *Megner and Gumbel*, 2009; *Zhang et al.*, 2022) throughout PMC altitude range, and ice particles grow predominantly in situ with negligible sedimentation. From the CMN perspective, mesospheric H_2O is modulated by a bottom-up process termed cold-trap effect (*Zhang et al.*, 2025a; *Zhang et al.*, 2025c). In the summer polar region, continuous solar UV radiation photolyzes

https://doi.org/10.5194/egusphere-2026-2688
Preprint. Discussion started: 11 June 2026

H_2O at the mesopause, resulting in extremely low H_2O concentrations above 90 km. This photolytic loss is balanced by upward H_2O transport from below, creating a sharp vertical H_2O gradient between 80 and 90 km. In December, the upwelling creates hydration below PMCs and induces low temperatures via adiabatic cooling, which enhance ice particle growth. The ice growth consumes H_2O faster than upwelling supplies it, so that dehydration occurs above PMCs because the solar UV photolysis loss is no longer balanced by upward transport. Meridional winds transport the hydration towards equator and winter hemisphere, in other words, cold-trap effect serves to protect H_2O from being immediately photolyzed by solar UV at summer polar mesopause and allows H_2O to influence ozone chemistry on global scale.

A key, testable distinction between the two frameworks lies in their predictions for weak-PMC conditions. The freeze-drying effect, in which dehydration is causally prior to hydration, predicts that hydration and dehydration are coupled. The cold-trap effect, in which hydration is driven directly by upwelling while dehydration requires sufficiently vigorous ice growth, predicts that when PMCs are weak, hydration can occur without accompanying dehydration. November and May, with their weak PMCs, offer a critical test of these competing predictions.

1.3 Mesospheric ozone chemistry

A secondary ozone maximum peaks at 90-95 km in the upper mesosphere (*Hays and Roble*, 1973; *Kaufmann et al.*, 2003), formed by the three-body recombination $O+O_2+M \rightarrow O_3+M$, favored by the low temperatures in this region (*Smith and Marsh*, 2005). Daytime O_3 is rapidly photolyzed, while nighttime O_3 is destroyed mainly by reactions with hydrogen ($H+O_3 \rightarrow OH+O_2$) and atomic oxygen ($O+O_3 \rightarrow 2O_2$) (*Zhu and Kaufmann*, 2018). The secondary ozone maximum exhibits strong seasonal dependence, with peak mixing ratio in winter when reduced sunlight minimizes photolysis and lower H_2O limits H availability. The interaction between odd oxygen ($O_x = O + O_3$) and odd hydrogen ($HO_x = H + OH + HO_2$) is central to MLT chemistry, with the HO_x catalytic cycle being the main loss process for O_x (*Kulikov et al.*, 2018a; *Kulikov et al.*, 2018b). The ozone photochemical equilibrium assumption links O_x and HO_x concentrations (*Kulikov et al.*, 2019). Meridional transport of H_2O from summer to winter hemisphere enhances ozone destruction via HO_x catalysis (*Marsh et al.*, 2003). O_3 and O contribute significantly to the mesospheric energy budgets through heating, chemical heating, and infrared cooling (*Mlynczak and Solomon*, 1993; *Ramesh et al.*, 2015). The total heating rate of O and O_3 is approximately 10 K day^{-1} on a global and annual mean basis (*Mlynczak et al.*, 2018), making O_x a potentially important driver of temperature interannual variability near mesopause.

Through the cold-trap effect, PMCs function as an upstream dam that regulates global H_2O distribution above 80 km, and potentially govern the HO_x–O_x chemistry across the MLT. The hydration below PMCs increases HO_x and reduces O_x near 83 km (*Murray and Plane*, 2005), while the dehydration above PMCs depletes H and enhances O_3 above ~90 km (*Siskind et al.*, 2008; *Siskind et al.*, 2018). Adiabatic cooling by upwelling also enhances O_3 through temperature-dependent ozone kinetics, with colder temperatures accelerating the three-body recombination reaction and suppressing the loss reactions (*Smith et al.*, 2018). In December, both dehydration-driven H depletion and adiabatic cooling contribute to O_x

https://doi.org/10.5194/egusphere-2026-2688
Preprint. Discussion started: 11 June 2026

enhancement above PMCs, making their relative contributions difficult to disentangle (*Zhang et al.*, 2025c). In November, if dehydration is indeed absent, the thermal pathway would be isolated, allowing temperature-dependent ozone kinetics to be studied independently of the complicating effects of H depletion.

1.4 Mesospheric climate

Polar mesospheric temperatures are dominated by the annual oscillation, driven by adiabatic cooling of upwelling in summer and warming of downwelling in winter. In contrast, tropical mesospheric temperatures exhibit a semi-annual oscillation, with maximum near the equinoxes at 85 km and near the solstices at 75 km (*Xu et al.*, 2007). Semi-annual oscillation signals are also prominent in tropical zonal winds (*Kishore Kumar et al.*, 2014), H_2O (*Gattinger et al.*, 2013; *Lossow et al.*, 2008), O_3 (*Lee and Wu*, 2020), and O (*Gu et al.*, 2022). The interannual variability of mesospheric temperatures has traditionally been attributed primarily to the 11-year solar cycle and CO_2-induced cooling (*Beig*, 2011a; *Beig*, 2011b). The CO_2-induced cooling trend is the outcome of CO_2 infrared emission toward out space (*Laštovička*, 2017) as well as the requirement of MLT energy conservation (*Mlynczak et al.*, 2024), and has been estimated at -0.5 to -1.0 K per decades (K/dec) from SABER data (*Bailey et al.*, 2021; *Das*, 2021; *Mlynczak et al.*, 2022; *Zhao et al.*, 2020). Solar cycle signals of 2-4 K per 100 solar flux unit are commonly extracted alongside the CO_2 trend. However, both solar and CO_2 signals are notably absent in the summer polar mesopause, a phenomenon attributed to a compensating dynamical effect (*Karlsson and Kuilman*, 2018) or a shrinking effect (*Bailey et al.*, 2021; *Lübken et al.*, 2013). Critically, the widely used multiple linear regression framework for extracting solar and CO_2 signals does not account for the internal variability of mesospheric dynamics.

Recent work has established that a bottom-up mechanism, namely the "upwelling—H_2O(H)—O_3(O)—T90" chain, drives substantial interannual variability in the MLT (*Zhang et al.*, 2025b; *Zhang et al.*, 2025c). This mechanism produces an interhemispheric anti-symmetric climate pattern during solstice months and a symmetric pattern during equinox months. November and May, as the transition months between these two regimes, offer a unique window into seasonal evolution of mesospheric climate organization.

This study addresses three questions: (1) What is the spatial pattern of interannual variability in H_2O, H, O_3, O, and temperature in the MLT during November and May? (2) What anomalous meridional circulation structure generates this pattern? (3) How do PMCs and ozone chemistry operate under these unique transitional conditions, and what do they reveal about the competing PMC microphysical framework?

https://doi.org/10.5194/egusphere-2026-2688
Preprint. Discussion started: 11 June 2026

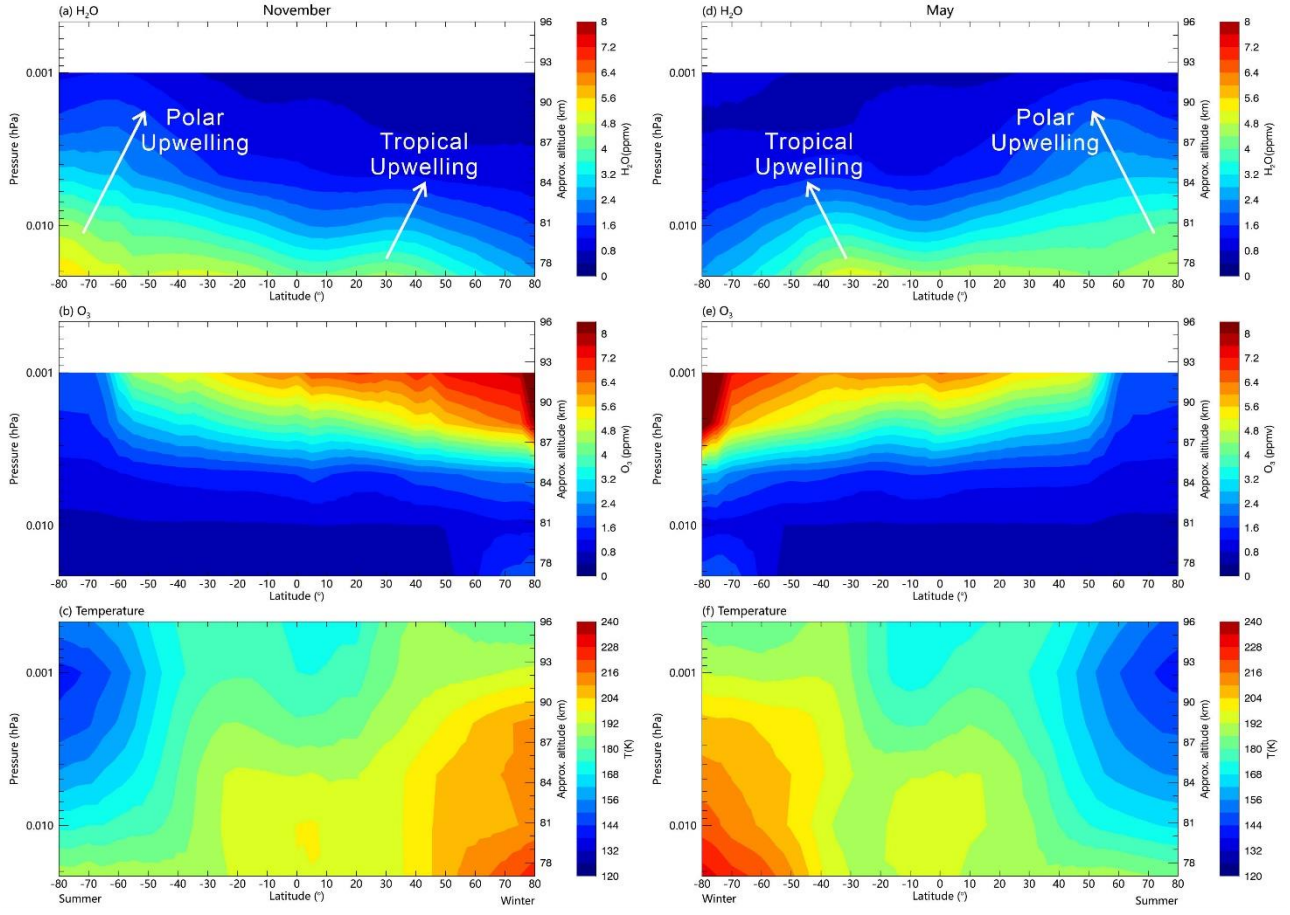

Figure 1. Climatology of water vapor mixing ratio, ozone mixing ratio, and temperature in the upper mesosphere for November (left) and May (right). Data are monthly means from MLS/Aura observations for 2004-2025.

2 Data and method

2.1 Multi-satellite data

This study utilizes measurements from two satellite instruments. The Microwave Limb Sounder (MLS) aboard NASA's Aura satellite, launched in July 2004, provides global atmospheric measurements between 82°N and 82°S (*Jiang et al.*, 2007). MLS delivers vertical profiles of H_2O (0.001 hPa top level recommended, 7~9 km vertical resolution, 30% precision), O_3 (0.001 hPa, 5~7 km, 35%), and temperature (0.00046 hPa, 6~12 km, 3 K). Daily mean values were generated by averaging ascending (01:30 local time) and descending (13:30 local time) orbits, and zonal (5° gridded) monthly means were used for interannual variability studies. Figure 1 shows the climatology of H_2O, O_3, and temperature in November from MLS.

The Sounding of the Atmosphere using Broadband Emission Radiometry (SABER) instrument aboard the Thermosphere, Ionosphere, Mesosphere Energetics, and Dynamics (TIMED) satellite was launched in December 2001.

https://doi.org/10.5194/egusphere-2026-2688
Preprint. Discussion started: 11 June 2026

SABER's limb scan provides latitude coverage that alternates between 83°N to 52°S (October) and 52°N to 83°S (December) due to its 60-day yaw cycle, but in November only the data between 52°S and 52°N are available (*Liu et al.*, 2024; *Russell et al.*, 1999). This 60-day yaw cycle allows interannual comparison by maintaining stable latitude and local time coverage for a given month across different years. We used TIMED/SABER version 2.07 data between 0.01 and 0.003 hPa from 2002 to 2023, including temperature (*Remsberg et al.*, 2008), ozone (*Rong et al.*, 2009; *Smith et al.*, 2013), atomic oxygen (*Mlynczak et al.*, 2013; *Mlynczak et al.*, 2018), and atomic hydrogen (*Mlynczak et al.*, 2014).

2.2 The T80 index: definition and justification

Direct measurements of vertical winds in the mesosphere remain unavailable in the form of continuous long-term records. We therefore employ a temperature-based proxy for the intensity of mesospheric upwelling on interannual timescales, the T80 index, defined as the zonal-mean temperature near 80 km. For summer polar upwelling, $T80_S$ is evaluated at ~80° latitude in the summer hemisphere (*Zhang et al.*, 2025c); for tropical upwelling, $T80_W$ is evaluated at ~20° latitude in the tropical region (*Zhang et al.*, 2025b). A lower T80 value indicates stronger upwelling (and thus stronger adiabatic cooling).

The choice of 80 km altitude is motivated by the following considerations. (1) Ozone concentrations are extremely low at this altitude, so radiative and chemical heating are negligible; temperature at this level is dominated by adiabatic processes. (2) The T80 index exhibits substantial interannual variability that dominates over long-term trends. In December, $T80_S$ over the summer pole has an interannual standard deviation of ~5.1 K, greatly exceeding its trend of ~1.5 K/dec (*Zhang et al.*, 2025c). (3) Because upwelling intensity is coupled to meridional circulation through mass continuity, the T80 index serves as a diagnostic of the associated meridional transports. (4) The steep vertical gradient of H_2O at ~80 km ensures that variations in upwelling efficiently modulate H_2O transport. This produces a robust negative T80-H_2O correlation, linking the T80 index to HO_x and O_x chemistry on a global scale. (5) Satellite temperature measurements near 80 km show high cross-platform consistency (*García-Comas et al.*, 2014), facilitating multi-instrument analysis. We emphasize that the T80 index captures anomalous upwelling and the accompanying anomalous meridional circulations, rather than the climatological mean residual circulation.

2.3 Bottom-up control mechanism framework

Our analysis framework examines the responses of mesospheric variables (H_2O, H, O_3, O, and T90) to upwelling on interannual timescales through the bottom-up mechanism established in our preceding works (*Zhang et al.*, 2025b; *Zhang et al.*, 2025c). This "upwelling—H_2O(H)—O_3(O)—T90" chain operates as follows. Upwelling transports H_2O vertically, modulating H (produced by H_2O photolysis). H acts as the primary catalyst for O_3 destruction, so O_3 varies inversely with H_2O. O varies in phase with O_3 due to the ozone photochemical equilibrium assumption. Finally, the total radiative and chemical heating of O and O_3 affects temperatures near 90 km. The sensitivity of chemical constituents and temperatures to the T80 index is quantified by linear regression of their monthly zonal-mean anomalies against T80 index anomalies.

https://doi.org/10.5194/egusphere-2026-2688
Preprint. Discussion started: 11 June 2026

3 Results

3.1 The bottom-up mechanism driven by the summer polar upwelling

3.1.1 Summer high-latitude response to $T80_S$

A distinctive feature of November is the PMC behavior and the associated H_2O redistribution, setting it apart from December. The correlation between $T80_S$ and H_2O above PMCs is statistically insignificant (R = -0.21, Fig. 2a), indicating the absence of detectable dehydration. Meanwhile, the correlation between $T80_S$ and H_2O below PMCs remains significantly negative (Fig. 3a), confirming that hydration persists. This "hydration-without-dehydration" configuration contrasts sharply with December, when strong PMCs produce both hydration below and dehydration above (*Zhang et al.*, 2025c).

The contrasting behavior carries distinct chemical consequences. As shown in Figure 4, the nighttime H atom in November is negatively correlated with the T80 index in both the SH and NH between 52°S and 52°N. In contrast, *Zhang et al.* (2025c) showed that the H in December is only negatively correlated with the T80 index in the NH but is insensitive in the SH (Fig. 4 therein). The absence of dehydration in November thus fundamentally alters the variability of H, which has direct implications for O_x chemistry. In December, both low temperatures and dehydration-driven H depletion contribute to O_3 enhancement above PMCs, making it difficult to disentangle their relative contributions. November—characterized by hydration but no dehydration—effectively eliminates the influence of the dehydration pathway, thereby allowing the temperature-dependent ozone kinetics to be studied in isolation.

The ozone response in the summer polar region confirms this interpretation. In the summer polar region, O_3 at 0.001 hPa is negatively correlated with $T80_S$ (R = -0.74, Fig. 2b), indicating that stronger upwelling (lower $T80_S$) is associated with higher O_3. This relationship is captured in the spatial pattern of O_3 sensitivity to $T80_S$ (Fig. 3b), which shows a coherent region of negative sensitivity extending from the summer pole to approximately 55°S. In addition, using SOFIE/AIM observations at ~70° S during 2007–2013, *Zhang et al.* (2025c) has showed that the daily time series of O_3 at 90 km is negatively correlated with $T80_S$ throughout the PMC season (Fig. 6 therein), thus this work did not replot the SOFIE O_3 responses in November.

The O_x enhancement driven by adiabatic cooling does not heat the same altitude where it is produced. Rather, the upwelling that causes the cooling also transports O and O_3 upward. The corresponding O_3–T90 correlation is positive (R = 0.80, Fig. 2c), consistent with radiative and chemical heating of O_3 influencing temperatures. The observed sensitivity of $T90_S$ to $T80_S$ is ~0.6 K K^{-1} (R = -0.92, Fig. 2d). In December, when dehydration is also active, the O_x increase is further amplified by H depletion, leading to a stronger $T90_S$ response of ~1 K K^{-1} (*Zhang et al.*, 2025c). In November, the absence of dehydration isolates the thermal pathway, yielding the weaker but still significant response.

3.1.2 Equatorial response to $T80_S$

The summer polar upwelling influences not only the summer polar mesopause but also the equatorial region. The polar-driven anomalous meridional circulation flows from the summer pole toward the equator, transporting hydration and its chemical consequences into the tropics.

https://doi.org/10.5194/egusphere-2026-2688
Preprint. Discussion started: 11 June 2026

MLS observations confirm this chain. The O_3 in the equatorial region is positively correlated with $T80_S$ (R = 0.83, Fig. 2f), indicating that stronger polar upwelling (lower $T80_S$) is associated with lower equatorial O_3. The corresponding O_3–$T90_{EQ}$ correlation is positive (R = 0.84, Fig. 2g), and $T90_{EQ}$ is positively correlated with $T80_S$ (R = 0.83, Fig. 2h), confirming that stronger polar upwelling leads to lower equatorial mesopause temperatures. The spatial pattern of MLS observations (Fig. 3) and SABER observations (Fig. 4) corroborate this picture. The consistent phasing of equatorial H_2O, H, O_x, and $T90_{EQ}$ across both MLS and SABER datasets supports the view that the bottom-up mechanism drives the equatorial climate in November, analogous to the equatorial climate in December (*Zhang et al.*, 2025c). The equatorial response is further shaped by the dynamical coupling between the polar and tropical upwellings. The poleward flow from the summer polar region is compensated by subsidence at low latitudes, so that $T80_{EQ}$ is weakly negatively correlated with $T80_S$ (Figs. 3c and 4d). This adiabatic warming from the compensating downwelling may affect the tropical upwelling ($T80_W$) in the winter hemisphere.

The pictures in May (Figs. 5–7) are mirrored to those of November (Figs. 2-4), further corroborating the bottom-up mechanism.

https://doi.org/10.5194/egusphere-2026-2688
Preprint. Discussion started: 11 June 2026

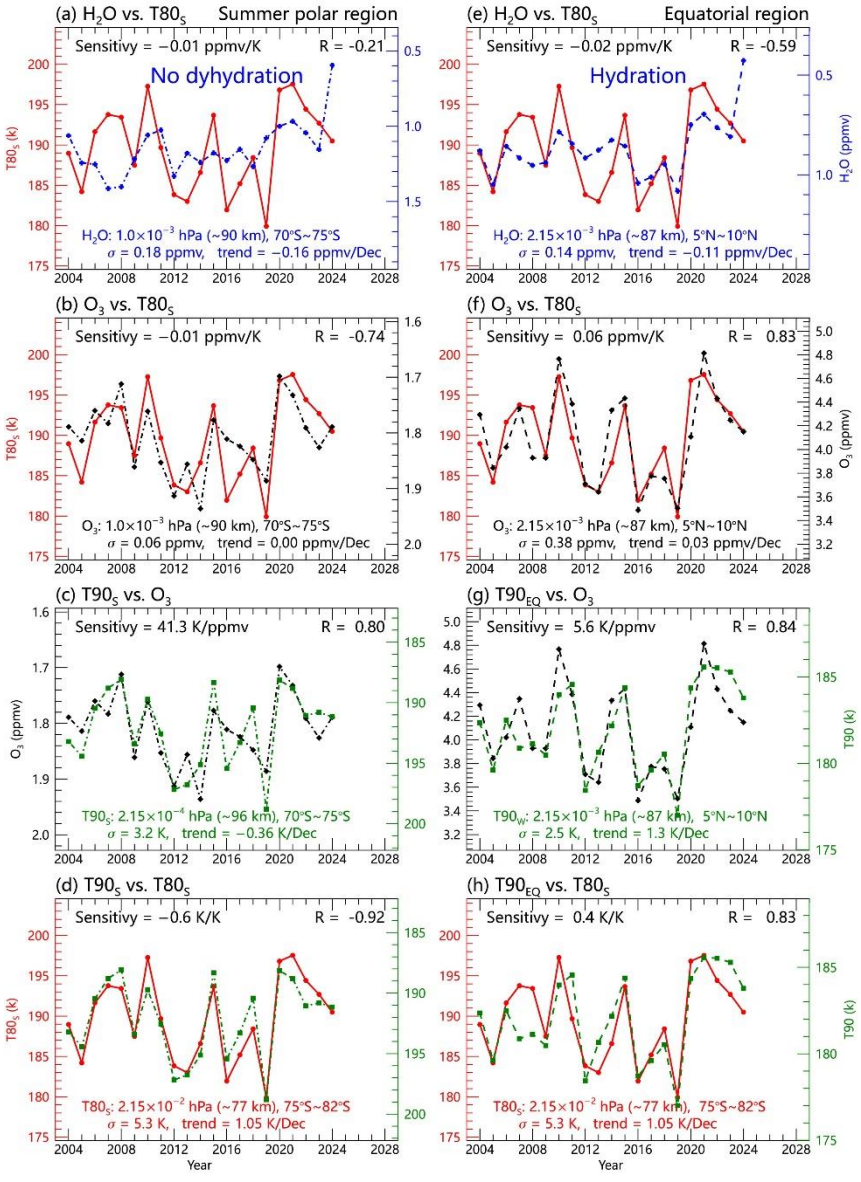

Figure 2. Interannual relationships between $T80_S$ upwelling index and mesospheric (a, e) H_2O, (b, f) O_3, and (d, h) T90 in November, showing the anti-phase response between the (left) summer polar region and (right) equatorial region. Panels (c, g) show the corresponding O_3-T90 correlations. All data are monthly and zonal means from MLS/Aura observations during 2004-2024. Correlation coefficients (R), sensitivities, standard deviations (σ), and trends are derived from linear regression analysis. The negative H_2O-$T80_S$ correlation in the equatorial region indicates hydration driven by upwelling, while the statistically insignificant corelation in the summer polar region indicates the absence of detectable dehydration. This pattern highlights the "upwelling—H_2O—O_3—T90" bottom-up chain and the distinct H_2O responses under weak PMC conditions.

https://doi.org/10.5194/egusphere-2026-2688
Preprint. Discussion started: 11 June 2026

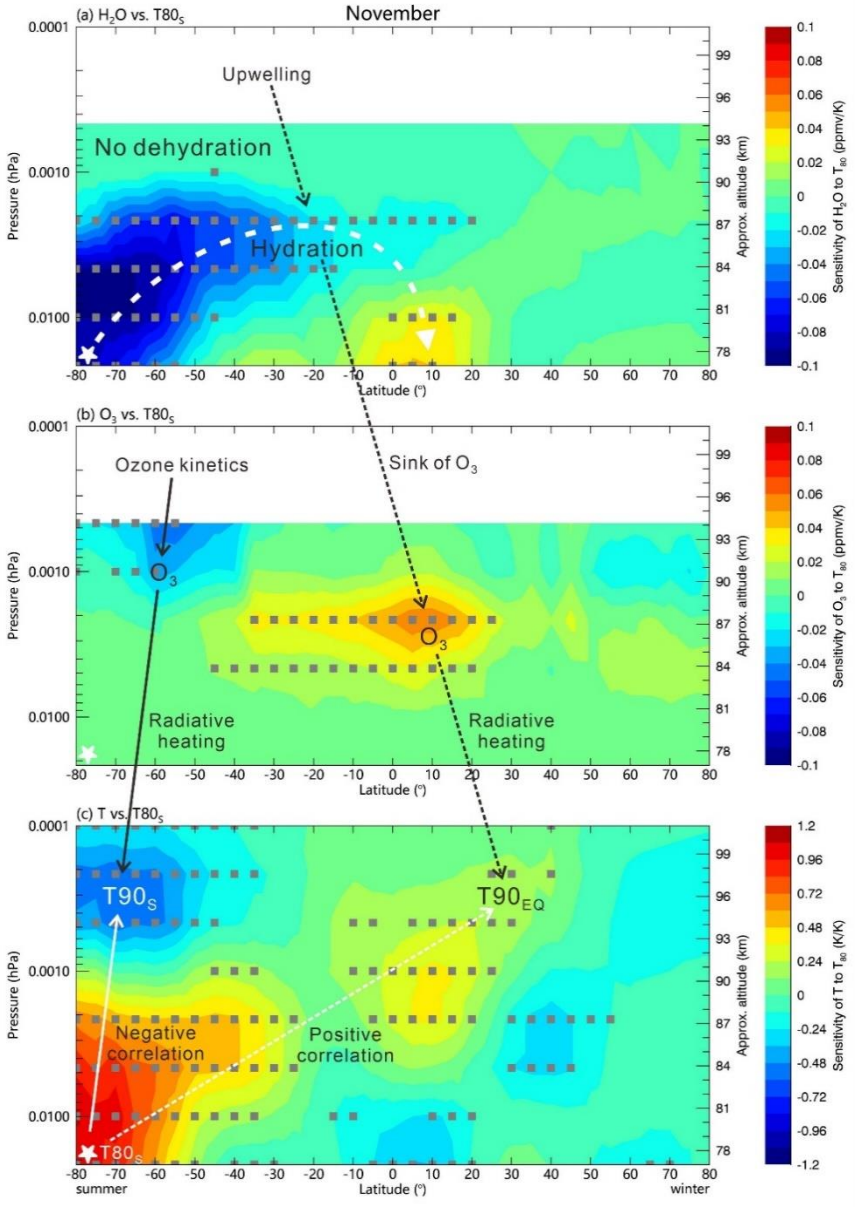

Figure 3. Height-latitude response pattern driven by summer polar upwelling ($T80_S$) in November. Spatial sensitivities of (a) H_2O, (b) O_3, and (c) temperature to $T80_S$, derived from MLS/Aura data (2004-2024), illustrate the bottom-up mechanism. (a) H_2O hydration extending from the summer pole to the equator (blue), with no significant dehydration over the summer polar mesopause. Dashed white lines mark H_2O transport pathways, suggestive of anomalous circulations. (b) a corresponding anti-phase O_3 response (increase over the summer polar mesopause, decrease in the tropics). (c) a resultant T90 structure of cooling (tropics) and warming (above summer polar mesopause and winter mid-latitudes). Gray points denote areas exceeding the 0.95 significance level. The white stars mark the locations (0.0215 hPa, 75°S-82°S) of the $T80_S$ index.

https://doi.org/10.5194/egusphere-2026-2688
Preprint. Discussion started: 11 June 2026

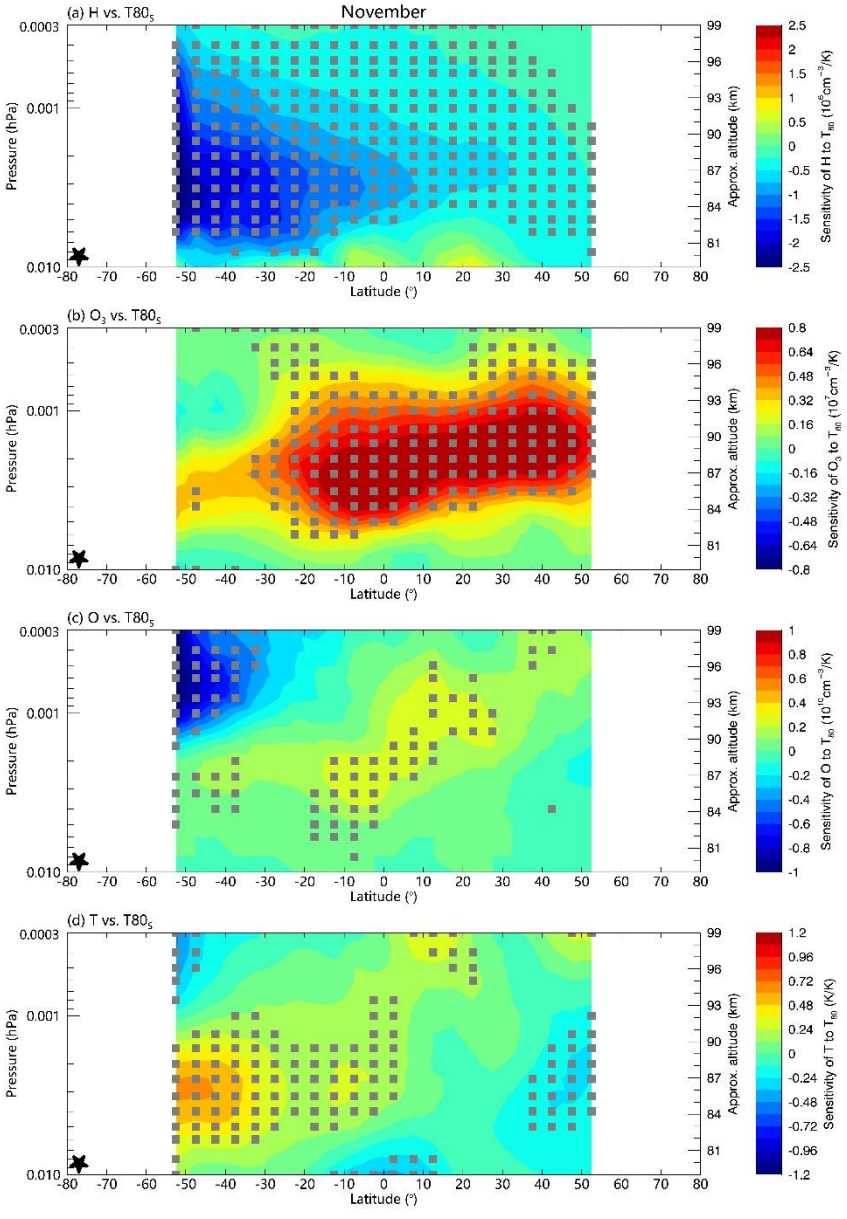

Figure 4. As in Fig. 3, but for SABER observations (2004-2023) of (a) H, (b) O_3, (c) O, and (d) temperature sensitivity to the $T80_S$ upwelling index (black stars) in November. The $T80_S$ index is from MLS observations, as in Fig. 2. (a) H shows a negative sensitivity in both hemispheres. (b) O_3 is significantly sensitive in the equatorial region but insensitive at 52°S above 0.001 hPa. (c) O responses significantly at both 52°S and the equatorial region, with opposite signs at the two locations. (d) Temperature responses is negative in the summer polar region ($T90_S$) and positive in the equatorial region ($T90_{EQ}$). Gray dots mark the 0.95 significance level.

https://doi.org/10.5194/egusphere-2026-2688
Preprint. Discussion started: 11 June 2026

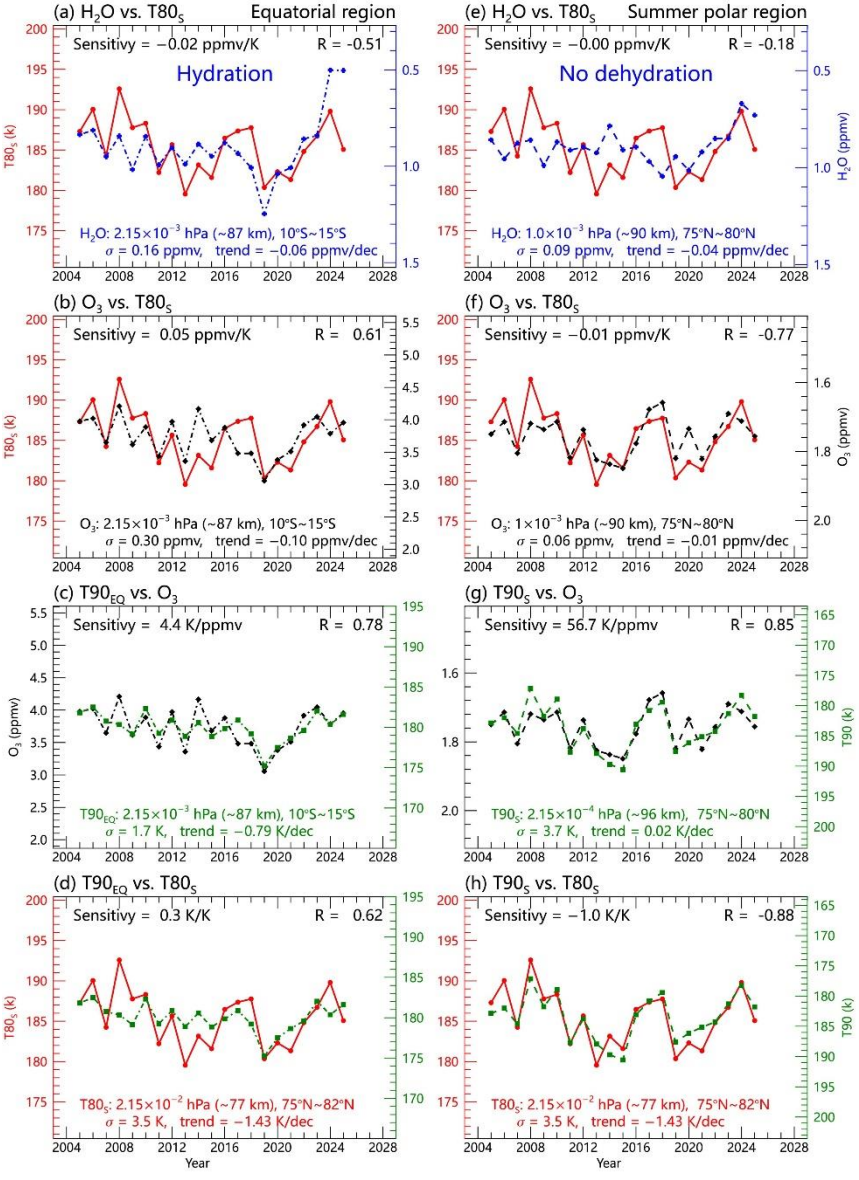

Figure 5. As in Fig. 2, but for May. All data are monthly and zonal means from MLS/Aura observations during 2005-2025.

https://doi.org/10.5194/egusphere-2026-2688
Preprint. Discussion started: 11 June 2026

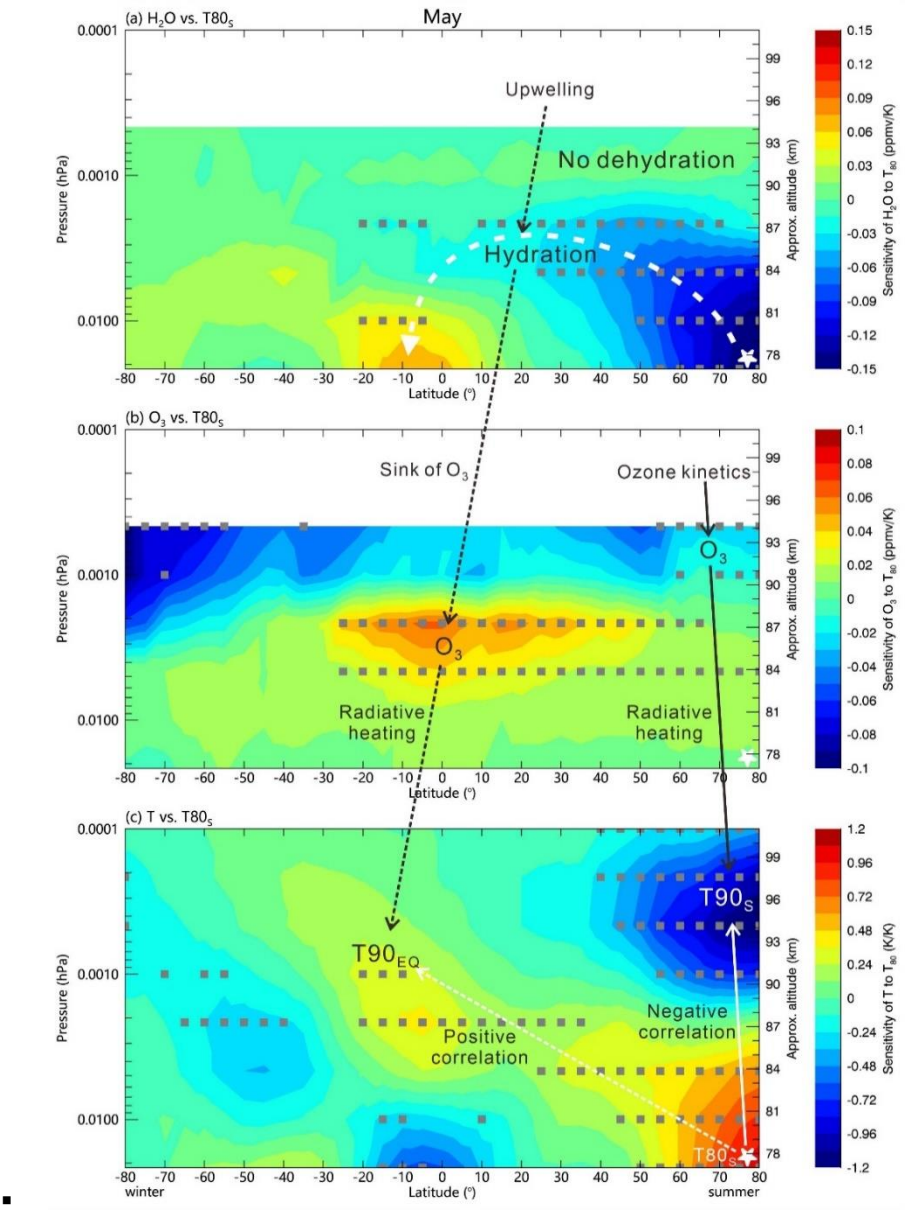

Figure 6. As in Fig. 3, but for May, showing mirror responses in May analogous to November. All data are from MLS/Aura observations during 2005-2025.

https://doi.org/10.5194/egusphere-2026-2688
Preprint. Discussion started: 11 June 2026

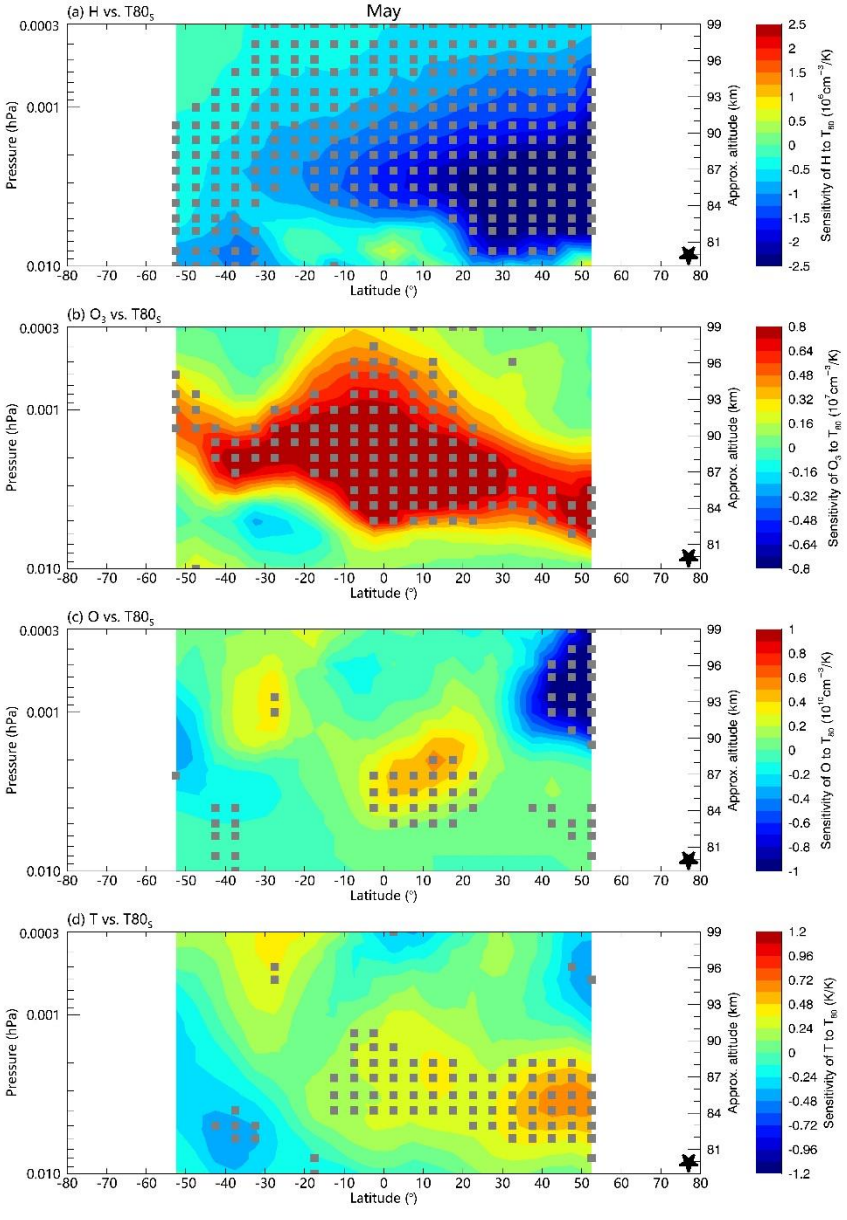

240

Figure 7. As in Fig. 4, but for May. All data are from SABER observations during 2005-2023. The $T80_S$ index (black stars) is from MLS.

https://doi.org/10.5194/egusphere-2026-2688
Preprint. Discussion started: 11 June 2026

3.2 The bottom-up mechanism driven by the tropical upwelling

In the winter hemisphere, the climate variability is governed by the tropical upwelling. Figure 8 shows the time series of key variables in the "upwelling—H_2O—O_x—T90" chain for the winter hemispheres in May (left panels) and November (right panels). $T80_W$ (at ~20° N, 0.01 hPa) exhibits an interannual standard deviation of ~1.7 K in November, considerably smaller than that of T80s (~5.1 K). The weaker variability of the tropical upwelling indicates that the winter hemisphere branch of the double-celled circulation is less energetic than its summer hemisphere counterpart.

Figs. 8a and 8e show that $T80_W$ is negatively correlated with H_2O in the winter hemispheres in May and November, confirming that tropical upwelling transports H_2O upward and poleward. Figs. 8b and 8f show the corresponding anti-correlation between H_2O and O_3, and Figs. 8c and 8g show the positive O_3–$T90_W$ coupling. The complete chain is summarized in Figs. 8d and 8h, where $T90_W$ is positively correlated with $T80_W$.

The spatial structure of the winter hemisphere response is shown in Figs. 9 and 10. The tropical upwelling drives an anomalous meridional circulation that transports H_2O from low latitudes toward the winter pole (Fig. 9a–b). This hydration reduces O_3 at mid-to-high latitudes in the winter hemisphere (Fig. 9c–d), and the resulting reduction in O_x heating leads to lower $T90_W$ (Fig. 9e–f). The SABER data (Fig. 10) independently confirm this chain, showing consistent responses of H, O_3, O, and $T90_W$ to $T80_W$.

The mechanism governing the winter hemisphere follows the same "upwelling—H_2O(H)—O_x—T90" chain that operates in the equatorial region. The winter hemisphere climate in November and May is, in essence, analogous to the symmetric climate pattern of equinox months (*Zhang et al.*, 2025b), with the tropical upwelling playing the role of dynamical driver.

https://doi.org/10.5194/egusphere-2026-2688
Preprint. Discussion started: 11 June 2026

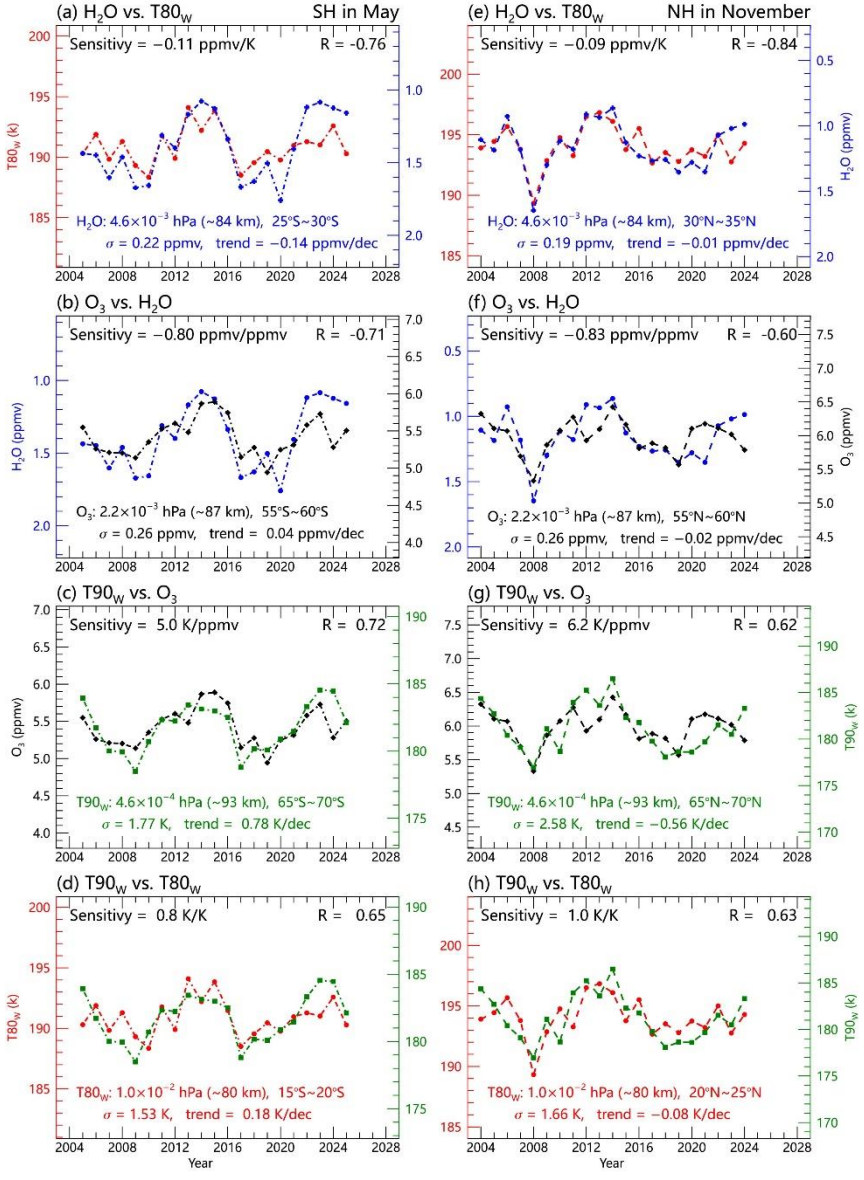

265 **Figure 8.** Time series of key variables in the "upwelling—H_2O—O_3—T90" chain for the winter hemisphere in (Left) November and (right) May. Tropical upwelling is indicated by the $T80_W$ index. (a, e) Interannual variations of $T80_W$ (~80 km, red) and H_2O (~83 km, blue). (b, f) Anti-correlation between H_2O (~83 km, blue) and O_3 (~87 km, black). (c, g) Correlation between O_3 (~87 km, black) and $T90_W$ (~93 km, green). (d, h) Coupling between low-latitude $T80_W$ (~80 km, red) and mid-to-high-latitude $T90_W$ (~93 km, green). Pressure levels, latitudes, standard deviations (σ), and long-term trends 270 of variables are given in each panel. All data are monthly and zonal means from MLS/Aura observations during 2004-2025. This pattern shows that tropical upwelling governs the winter-hemisphere climate, analogous to the equinox regime.

https://doi.org/10.5194/egusphere-2026-2688
Preprint. Discussion started: 11 June 2026

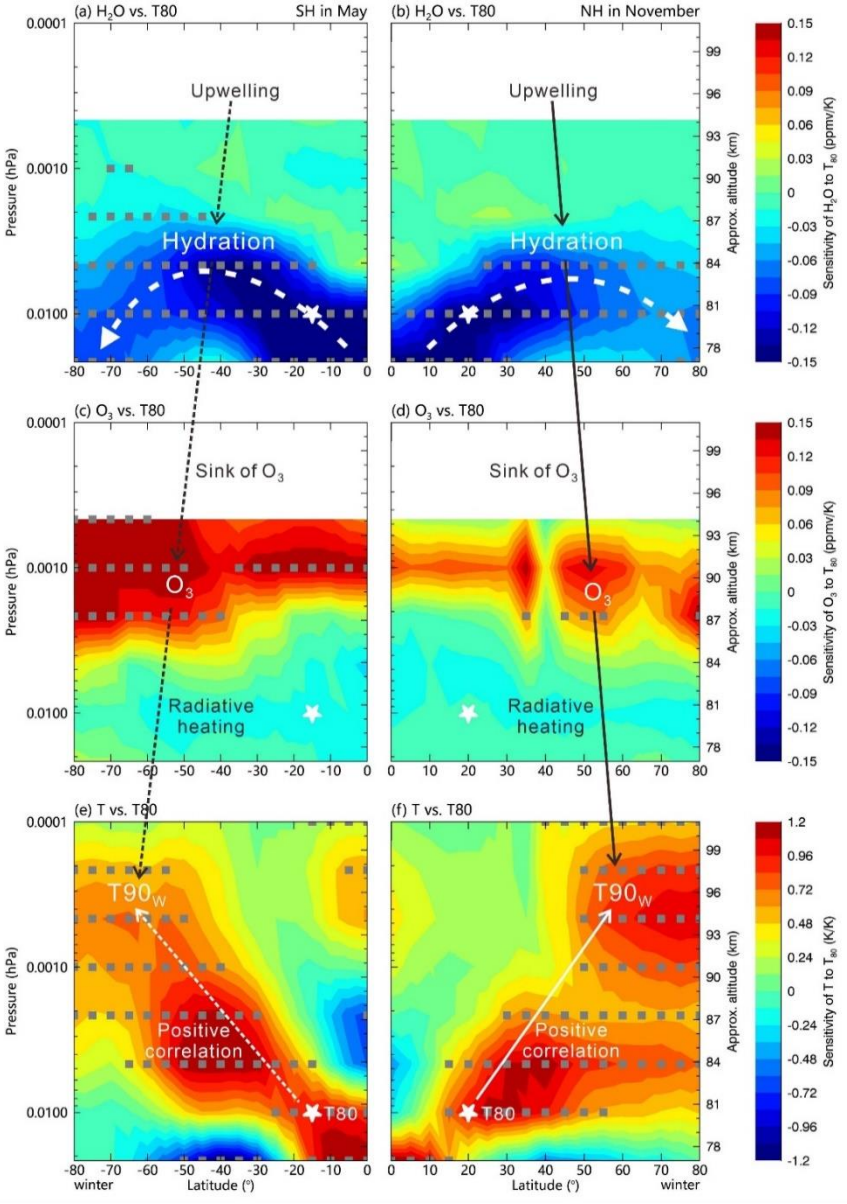

Figure 9. Height-latitude patterns of the sensitivity of (a, b) H_2O, (c, d) O_3, and (e, f) temperature to the $T80_W$ upwelling index (white stars at 15°–20°S in May and 20°–25°N in November on the 0.01 hPa level) in the winter hemisphere of (left) May and (right) November by MLS data (2004–2025). (a, b) Negative H_2O sensitivity indicates hydration driven by upward and poleward transport. Dashed white lines mark H_2O transport pathways, suggestive of anomalous circulations. (c, d) O_3 is regulated by $T80_W$ via the negative H_2O–O_3 correlation. (e, f) Positive correlations between low-latitude $T80_W$ and mid-to-high-latitude $T90_W$. Gray points denote the 0.95 significant level. This pattern shows that tropical upwelling independently forces the winter-hemisphere climate, completing the picture of the double-celled anomalous meridional circulation.

https://doi.org/10.5194/egusphere-2026-2688
Preprint. Discussion started: 11 June 2026

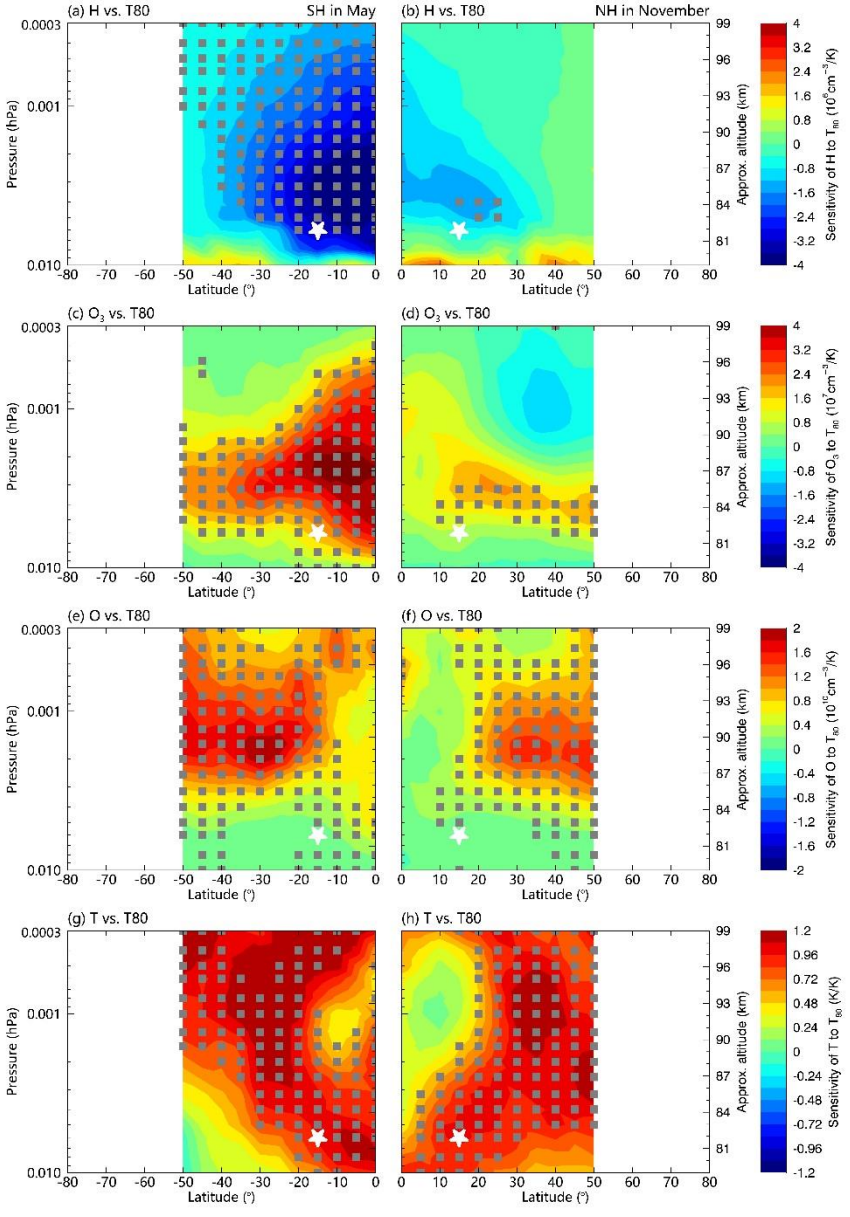

280

Figure 10. As in Fig. 9, but for SABER observations (2002–2023) of (a, b) H (c, d) O_3, (e, f) O, and (g, h) temperature sensitivity to the $T80_W$ upwelling index (white stars) in the winter hemisphere of (left) May and (right) November. The $T80_W$ index is evaluated at 15°–20°S/N on the 0.006 hPa level from SABER temperature data. (a, b) Negative H sensitivity reflects the upward transport of H_2O by tropical upwelling and subsequent photolysis. (c, d) The secondary ozone layer is
285 regulated by $T80_W$ through HO_x-driven catalytic loss. (e, f) O responds to $T80_W$ in phase with O_3, consistent with photochemical equilibrium. (g, h) Positive correlations between low-latitude $T80_W$ and mid-latitude $T90_W$ reflect the total heating of O and O_3. Gray points mark the 0.95 significant level.

https://doi.org/10.5194/egusphere-2026-2688
Preprint. Discussion started: 11 June 2026

4 Discussion

4.1 Seasonal evolution of circulation and the transition climate pattern

The double-celled anomalous meridional circulation that characterizes November and May can be understood as the natural transitional state between equinox and solstice circulation regimes (Figure 11). In October, upwelling is concentrated in the tropics, driving a symmetric anomalous meridional circulation from low latitudes toward both poles (*Zhang et al.*, 2025b). In November, summer polar upwelling intensifies in the SH. The polar-driven anomalous circulation, directed from the summer pole toward the equator, replaces the tropical-driven cell in the SH, while the tropical-driven cell persists in the NH. The result is a double-celled circulation: a pole-to-equator cell in the summer hemisphere and a tropics-to-pole cell in the winter hemisphere. The standard deviations of T80 (5.3 K for $T80_S$ in November vs. ~1.7 K for $T80_W$) reflect the amplitude of interannual variability, with polar upwelling variability being substantially stronger than tropical upwelling variability. By December, the summer polar upwelling dominates entirely, and the double-celled structure collapses into the classic pole-to-pole cell (*Zhang et al.*, 2025c). The May circulation is the mirrored counterpart, with the polar upwelling in the NH and the tropical upwelling in the SH.

This seasonal progression reveals that the November circulation is the natural bridge between two fundamentally different dynamical regimes. The double-celled structure is the defining dynamical feature of the transition months.

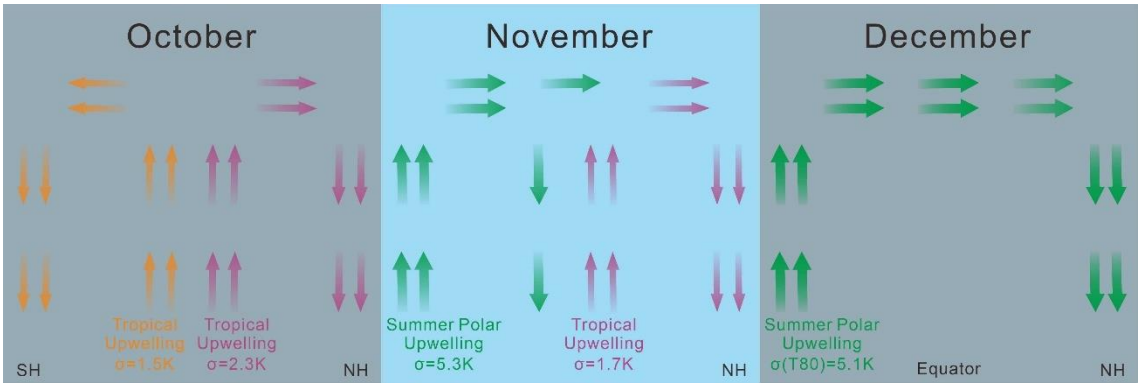

Figure 11. Schematic of seasonal evolution of upwelling-driven anomalous meridional circulations in the upper mesosphere from October to December. (Left) October: Symmetric anomalous circulation driven by tropical upwellings near 20°N/S, with poleward flow from the tropics to both hemispheres. (Middle) November: Emergence of a double-celled anomalous circulation. Summer polar upwelling intensifies in the SH, replacing the tropical-driven cell there, while the tropical-driven cell persists in the NH. (Right) December: Summer polar upwelling dominates entirely, establishing the classic summer-to-winter meridional circulation. Interannual standard deviations (σ) of the T80 index for each upwelling branch are shown, based on MLS data.

https://doi.org/10.5194/egusphere-2026-2688
Preprint. Discussion started: 11 June 2026

Through the bottom-up mechanism, the double-celled anomalous meridional circulations jointly organize temperatures and constituents into a coherent triple-structured pattern spanning the summer hemisphere high latitudes, the equatorial region, and the winter hemisphere high latitudes (Figure 12). As shown in Figs. 3c and 4d, the sensitivity of T90 to $T80_S$ exhibits a distinct three-zone structure: negative in the summer polar region ($T90_S$), positive in the equatorial region ($T90_{EQ}$), and weakly negative in the winter hemisphere mid-to-high latitudes ($T90_W$). This triple pattern arises from the superposition of two independent dynamical influences: the control of $T90_S$ and $T90_{EQ}$ by the summer polar upwelling, and the control of $T90_W$ by the tropical upwelling.

The weak negative correlation between $T90_W$ and $T80_S$ is a consequence of the weak anti-correlation between $T80_W$ and $T80_S$. Because the tropical upwelling region lies close to the equatorial subsidence zone, the compensating downwelling that warms $T80_{EQ}$ also influences $T80_W$, establishing a weak dynamical coupling between the two upwelling indices and transmitting the $T80_S$ signal into the winter hemisphere. However, given the limited length of the satellite record, it remains unclear whether this weak anti-correlation between the polar and tropical upwellings is a robust feature of the climate system or a sampling artifact.

The triple-structured pattern differs fundamentally from the interhemispheric anti-symmetric pattern of solstice months (*Zhang et al.*, 2025c) and the interhemispheric symmetric pattern of equinox months (*Zhang et al.*, 2025b). It demonstrates that the spatial organization of mesospheric climate variability evolves systematically with the seasonal cycle: from symmetric in October, through the transitional triple-structured pattern in November, to anti-symmetric in December. The May results mirror those of November, with the roles of the two hemispheres interchanged.

The magnitude of the dynamical variability far exceeds that attributable to long-term trends. The standard deviation of $T80_S$ in November is ~5.3 K, whereas its linear cooling trend is only ~1.1 K/dec (Fig. 2). This order-of-magnitude difference is mirrored in the key response variables: the interannual standard deviations of H_2O, O_3, and T90 consistently surpass their respective trends by a wide margin (Figs. 2, 5, 8), underscoring that internal dynamical variability, rather than long-term externally forced trends, dominates the interannual behavior of these fields. Furthermore, the spatial structure of the observed variability—with distinct, oppositely signed responses in three latitudinal zones—is incompatible with the expected fingerprints of globally uniform solar or CO_2 forcing, which would produce spatially coherent temperature and compositional responses across the globe. Neither the 11-year solar cycle nor the CO_2 increase can generate the interhemispheric symmetric pattern of equinox months, the interhemispheric anti-symmetric pattern of solstice months, or the triple-structured pattern reported here. A quantitative separation of the relative contributions of internal dynamical variability, solar forcing, and CO_2 forcing to mesopause climate extends beyond the scope of this paper and requires dedicated model experiments.

https://doi.org/10.5194/egusphere-2026-2688
Preprint. Discussion started: 11 June 2026

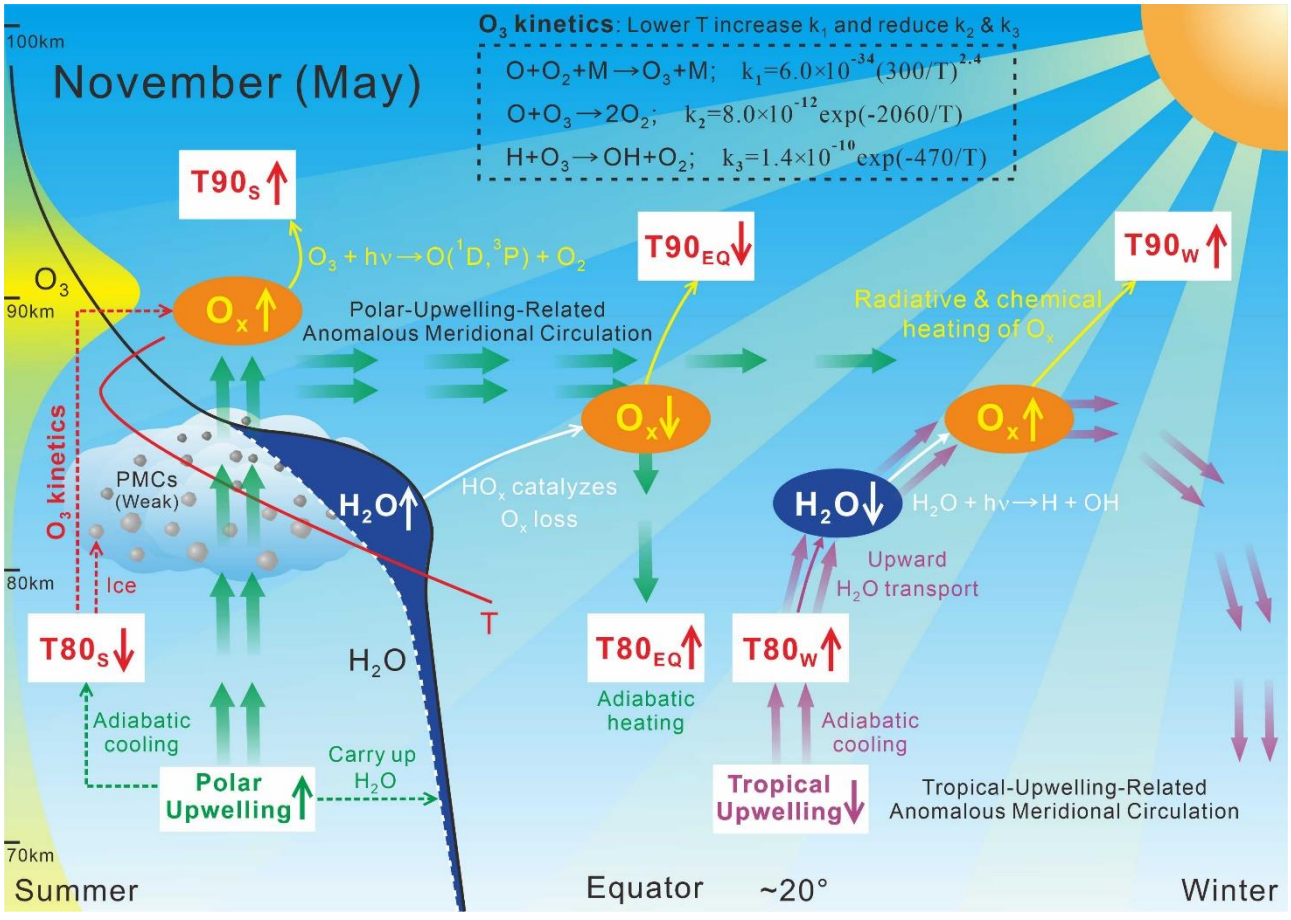

345 **Figure 12.** Schematic diagram of the bottom-up control mechanism in November and May, illustrating how summer polar upwelling and tropical upwelling jointly govern climate variability through coupled dynamical, microphysical, and chemical processes. Key pathways include: (1) Summer polar upwelling transport H_2O equatorward via the anomalous meridional winds. The resulting hydration increase H (via photolysis), which catalytically destroys O_3. Concurrent adiabatic cooling enhances O_3 through temperature-dependent ozone kinetics. O varies in phase with O_3 under photochemical equilibrium, and
350 the combined radiative and chemical heating of O and O_3 governs $T90_S$ and $T90_{EQ}$. (2) Tropical upwelling transports H_2O poleward in the winter hemisphere, where the subsequent H-driven ozone loss reduces O_3 and O, and the resulting decrease in O_x heating lowers $T90_W$.

https://doi.org/10.5194/egusphere-2026-2688
Preprint. Discussion started: 11 June 2026

4.2 Microphysics of transitional PMCs: evidence for the cold-trap effect

The "hydration-without-dehydration" configuration documented in Section 3.1.1 is a distinctive prediction of the cold-trap effect based on the CMN scheme (*Zhang et al.*, 2025a; *Zhang et al.*, 2025c). Within this framework, hydration and dehydration are driven by distinct physical mechanisms: hydration results directly from the upward transport of H_2O by upwelling, while dehydration requires ice particles to be sufficiently abundant to consume more H_2O than is delivered from below, thereby blocking net upward transport. When PMCs are weak—as in November—the ice-mediated blocking becomes ineffective and dehydration does not occur, even though upwelling continues to deliver H_2O to PMC altitudes, producing hydration. The recent simulations of *Vellalassery et al.* (2026) support this interpretation, showing that stronger vertical winds carry more H_2O to both the lower and upper parts of PMCs, and that ice growth alone cannot block the upward H_2O transport.

Independent observational support comes from *Hervig et al.* (2015), who used SOFIE measurements to systematically identify dehydration and hydration layers based on water vapor residuals relative to a carefully constructed PMC-free background. Notably, in their Fig. 3, strong hydration cases were found to be approximately 10 K warmer below 84 km than strong dehydration cases, yet temperatures above 84 km were nearly identical between the two categories. Within the CMN framework, this temperature structure finds a natural explanation. Hydration can occur under relatively weak upwelling (higher $T80_S$), in which case upwelling delivers H_2O to produce hydration below PMCs, but ice growth is insufficient to block upward transport and dehydration does not occur above. Dehydration cases, conversely, correspond to strong upwelling (lower $T80_S$), in which case ice growth consumes H_2O faster than upwelling can supply it, producing net dehydration above PMCs, while hydration still occurs below. Furthermore, *Hervig et al.* (2015) found that the column abundance of H_2O in ice layers often exceeded the combined H_2O changes in the dehydration and hydration layers (their Fig. 5). In the CMN framework, this imbalance is an expected consequence of the fact that the H_2O forming ice is supplied by upwelling from below, rather than being internally redistributed from the dehydration layer. The conventional assumption that ice water content should balance the sum of dehydration and hydration is not a necessary condition in the cold-trap effect framework.

We acknowledge that the observed "hydration-without-dehydration" pattern does not, by itself, logically falsify the conventional freeze-drying framework. One could argue that when PMCs are sufficiently weak, the mass of water redistributed by ice particle sedimentation may fall below the detection threshold of satellite instruments. However, the cold-trap framework offers a more parsimonious explanation for the seasonal transition from November (hydration-only) to December (hydration plus dehydration): as summer polar upwelling intensifies, the ice-mediated blocking of upward H_2O transport becomes progressively stronger. We emphasize that the freeze-drying effect and the cold-trap effect are not mutually exclusive; instead, they likely dominate on different spatial and temporal scales, and a complete understanding will benefit from the integration of both frameworks.

https://doi.org/10.5194/egusphere-2026-2688
Preprint. Discussion started: 11 June 2026

4.3 The isolated thermal pathway in polar ozone chemistry

The absence of dehydration above PMCs in November provides a unique opportunity to quantify the thermal contribution to polar mesopause ozone enhancement. SABER observations (Fig. 4) constrain the underlying chemical pathways. Fig. 4a shows that H at 52°S is negatively correlated with T80s in November, indicating that in the absence of dehydration, H is controlled directly by upwelling-driven H_2O transport. This is in marked contrast to December, where dehydration above strong PMCs depletes H_2O and renders H at 52°S insensitive to $T80_S$ (*Zhang et al.*, 2025c). Consequently, the O_3 enhancement in November cannot be explained by H depletion due to dehydration. Instead, it arises from the temperature dependence of ozone kinetics: colder temperatures accelerate the three-body recombination $O + O_2 + M$ and suppress the $H + O_3$ and $O + O_3$ loss pathways (*Smith et al.*, 2018).

The mesopause O_3 response at 52°S in November from SABER, however, is not statistically significant (Fig. 4b). This apparent inconsistency may arise because 52°S lies near the equatorward boundary of the O_3 response region, which MLS data show extends only to approximately 55°S (Fig. 3b). It is noteworthy, however, that the nighttime O at 52°S is sensitive to $T80_S$ (Fig. 4c) while the nighttime O_3 at the same latitude is not. Under nighttime conditions, if both H and O increase concurrently at 52°S in response to stronger upwelling (Figs. 4a, 4c), the simultaneous enhancement of the O_3 production term (proportional to O) and the primary loss terms (proportional to H and O) may result in a near-zero net O_3 change. Alternatively, the longer photochemical lifetime of O relative to O_3 may allow O perturbations to be transported to 52°S while O_3 perturbations are locally dissipated. These contrasting responses of O and O_3 at the same location are examined further in Section 4.4.

The mechanism described above addresses the interannual variability of ozone during November. On seasonal timescales, *Siskind et al.* (2018) used the WACCM-PMC model to demonstrate that dehydration due to PMC ice condensation leads to significant depletion of H above the summer polar mesopause, reducing the $H + O_3$ loss pathway and contributing to a local summertime O_3 maximum. Our results are complementary rather than contradictory: they show that on interannual timescales, and specifically during November when PMCs are weak and dehydration is absent, the O_3 variability is governed primarily by temperature-dependent ozone kinetics rather than by H depletion. The two mechanisms operate on different timescales (seasonal vs. interannual) and dominate under different PMC conditions (strong vs. weak). Together, they provide a more complete picture of how dynamics and chemistry interact to control polar mesopause ozone.

4.4 $T90_S$ variability: heating processes in the summer hemisphere

The positive correlation between O_3 and T90 (R = 0.80, Fig. 2c) is consistent with the hypothesis that radiative and chemical heating by O_x influences mesopause temperatures. However, the O_x enhancement driven by adiabatic cooling does not heat the air at the altitude where it is produced. The same upwelling that causes the cooling also transports O and O_3 upward, where the lower atmospheric density amplifies the temperature response to a given heating input. This non-local heat release constitutes a negative feedback that is fundamentally distinct in spatial character from the in situ negative feedback described

https://doi.org/10.5194/egusphere-2026-2688
Preprint. Discussion started: 11 June 2026

by *Grygalashvyly et al.* (2025), where chemical heating directly opposes the initial cooling at the same altitude. In our case, the feedback is non-local: chemical heating generated near 90 km is advected to higher altitudes by the very upwelling that initiated the cooling. These two modes of O_x–temperature coupling are complementary, with the non-local mode likely becoming important when vertical transport is strong.

We do not attempt a rigorous closure of the upper mesospheric energy budget, which requires dedicated modeling studies. Instead, we perform an order-of-magnitude check to confirm physical plausibility. Taking the global, annual mean total heating rate of O and O_3 of ~10 K day^{-1} (*Mlynczak et al.*, 2018) as a reference, and the observed ~4% K^{-1} sensitivity of O_x to $T80_S$ (not shown) as a representative perturbation, the corresponding change in the O_x heating rate is on the order of ~0.4 K day^{-1} K^{-1}. Given the 3-day lag between $T80_S$ and $T90_S$ reported by (*Zhang et al.*, 2025c), and the lower atmospheric density at T90 altitudes which amplifies the thermal response, an integrated heating effect of ~0.6 K K^{-1} (Fig. 2d) is physically plausible. We therefore interpret the O_x–T90 relationship as physically consistent with, though not definitively proving, the bottom-up mechanism.

A critical test of causation arises from the SABER observations at 52°S in November, where the nighttime O_3 and O exhibit different interannual variability. At this location, nighttime O_3 near 90 km shows no statistically significant response to $T80_S$ (Fig. 4b), yet nighttime O exhibits a robust anti-correlation with $T80_S$ ($R \approx -0.90$, Fig. 4c). This decoupling constitutes a natural experiment for evaluating the relative roles of O_3 and O in driving $T90_S$ variability. Critically, the anti-correlation between $T90_S$ and $T80_S$ at 52°S remains strong (Fig. 4d) despite the absence of a significant O_3 signal. If O_3 variations were the primary driver of $T90_S$, their disappearance at 52°S should weaken or eliminate the $T90_S$–$T80_S$ correlation. That the correlation persists strongly points to O as the dominant heating agent at high summer latitudes.

This inference is supported by independent evidence on the vertical structure of chemical heating. *Wu et al.* (2026) demonstrated that at low latitudes, nighttime chemical heating from the H + O_3 reaction (~4–5 K day^{-1}, prevailing below ~92 km) and the O + O + M recombination reaction (~5 K day^{-1}, prevailing above ~92 km) are comparable in magnitude. In the summer polar mesopause region, however, O_3 concentrations are drastically reduced by photolysis and strong HO_x-driven catalytic loss, while O remains abundant due to persistent daylight photolysis of O_2. The decoupling at 52°S, combined with the known vertical structure of heating rates, therefore supports the view that interannual variability in O, rather than O_3, is the primary driver of chemical heating variability at the high-latitude summer mesopause. We further note that the sensitivity of T90s to O_3 is 41.3 K/ppmv in November (Fig. 2c) and 56.7 K/ppmv in May (Fig. 5g). These unrealistically high values arise from the extremely low O_3 abundance at the summer polar mesopause and should not be interpreted as evidence of direct O_3 control over T90s. Rather, O varies in phase with O_3 through photochemical equilibrium (Figs. 4b, c), and the apparent high sensitivity of T90s to O_3 is a statistical artifact of this covariance. At 52°S the covariance breaks down, and O emerges as the more fundamental driver.

A purely dynamical mechanism could, in principle, contribute to the observed anti-correlation between $T80_S$ and $T90_S$. In the climatological mean, the summer polar residual circulation is characterized by upwelling below the mesopause, with a reversal to downwelling in the lower thermosphere above approximately 95–100 km (*Becker*, 2012). If intensified

https://doi.org/10.5194/egusphere-2026-2688
Preprint. Discussion started: 11 June 2026

upwelling at 80 km were accompanied by intensified downwelling at lower thermospheric altitudes on interannual timescales, adiabatic heating from the downwelling could produce a $T90_S$ increase that is dynamically rather than chemically driven. However, several considerations suggest that such a dynamical contribution is unlikely to dominate the $T90_S$ response. First, $T90_S$ (~0.001 hPa) lies within the upwelling branch of the residual circulation, well below the altitude where the reversal to downwelling is expected. Second, *Zhang et al.* (2025c) showed that $T90_S$ lags behind O_3 and $T80_S$ by approximately 3 days (Figure 8 therein), a timescale that is inconsistent with an instantaneous adiabatic response but consistent with the accumulation of chemical heating. Third, it remains unproven whether interannual variability of lower thermospheric downwelling is sufficiently coherent with that of mesospheric upwelling to produce a measurable $T90_S$ signal. These arguments weigh against a dominant role for dynamical heating, and we conclude that the available evidence favors a primarily chemical origin for $T90_S$ interannual variability.

The discussions above highlight that the O_x–T90 coupling involves multiple overlapping processes whose individual contributions remain to be fully quantified. While the statistical relationships we present are physically coherent and consistent with the bottom-up mechanism, a fully quantitative closure of the energy budget on interannual timescales, and a definitive separation of chemical and dynamical heating pathways, will require dedicated model experiments with resolved wave driving and interactive chemistry.

4.5 Limitations and open questions

While this study presents a coherent picture of the transitional mesospheric climate regime, several inherent limitations and open questions must be acknowledged to frame the scope of our conclusions and guide future research.

First, and foremost, while the key statistical relationships reported here are consistent and reproducible across multiple satellite datasets, they represent correlative rather than definitive causal evidence for the proposed bottom-up mechanism. Validation of the proposed causal chain will require explicit numerical simulations with coupled dynamics, microphysics, and chemistry.

Second, summer polar upwelling is known to be driven by gravity wave breaking, but the physical origins of tropical upwelling variability on interannual timescales remain unclear. The weak anti-correlation between the polar and tropical upwelling indices, while physically interpretable through mass flux conservation, requires confirmation with longer observational records or dedicated model simulations. Whether this coupling is a robust characteristic of the mesospheric circulation remains an open question.

Third, neither the conventional freeze-drying effect nor the cold-trap effect should be viewed as universally applicable. They likely dominate on different spatial and temporal scales, and a complete understanding of PMC-mediated H_2O redistribution will require the integration of both frameworks. The T80 index, introduced and formalized in this series of studies, may serve as a useful diagnostic for such integrative efforts.

Fourth, it should be noted that the O_x–T90 coupling is complex and involves multiple overlapping heating processes whose individual contributions remain to be fully quantified. While this study demonstrates coherent statistical relationships

https://doi.org/10.5194/egusphere-2026-2688
Preprint. Discussion started: 11 June 2026

among variables that strongly support the bottom-up mechanism, the O_x–T90 link should be regarded as physically consistent but not strictly quantitative in the present analysis. A fully quantitative closure of the energy budget on interannual timescales, disentangling the individual contributions of different heating reactions, is essential for future investigations.

5 Conclusion

This study has investigated the interannual variability of upper mesospheric climate during November and May, revealing a dynamical and chemical regime that is fundamentally distinct from those of solstice and equinox months. Our multi-satellite analysis establishes the following conclusions.

First, we identify a double-celled anomalous meridional circulation that characterizes the transitional months. Summer polar upwelling drives a pole-to-equator anomalous circulation, while tropical upwelling drives a tropics-to-winter-pole anomalous circulation. The two upwellings, diagnosed by the T80 index, exhibit weakly anti-correlated interannual variability, suggesting dynamical coupling associated with mass continuity. The May circulation pattern mirrors that of November with the hemispheric roles reversed. This double-celled structure represents the transitional state bridging the previously documented equinox and solstice circulation regimes (*Zhang et al.*, 2025b; *Zhang et al.*, 2025c), thereby completing the seasonal evolution picture of upwelling-driven anomalous circulations in the upper mesosphere.

Second, this double-celled circulation produces a triple-structured climate pattern. Through the bottom-up mechanism of "upwelling—H_2O(H)—O_x—T90", the summer polar upwelling simultaneously governs interannual variability in the summer polar region ($T90_S$) and the equatorial region ($T90_{EQ}$), with these two regions responding in antiphase. Meanwhile, the tropical upwelling governs variability in the winter hemisphere mid-to-high latitudes ($T90_W$). This partitioning of the upper mesosphere into three distinct latitudinal climate zones cannot be explained by the globally uniform external forcings (e.g., solar cycle, CO_2-cooling), indicating the dominant role of internal dynamics.

Third, the contrasting PMC behavior between November and December provides critical evidence for distinguishing between the conventional freeze-drying effect and the cold-trap effect. In November, weak PMCs allow hydration below the cloud layer via upwelling-driven transport, but ice growth is insufficient to block further upward water vapor transport, resulting in no detectable dehydration above. This "hydration-without-dehydration" configuration is a natural and distinguishing prediction of the cold-trap effect, in which hydration and dehydration are driven by separate physical mechanisms rather than being causally linked through particle sedimentation.

Fourth, the absence of dehydration above PMCs in November isolates the contribution of temperature-dependent ozone kinetics to polar mesopause ozone enhancement. In December, both adiabatic cooling and dehydration-driven H depletion contribute to enhanced O_x, making their relative roles difficult to disentangle. In November, however, the dehydration pathway is inoperative, and the observed O_x enhancement should arise primarily from ozone kinetics. This finding clarifies the chemical pathways that link upwelling to mesopause temperatures under different PMC conditions.

https://doi.org/10.5194/egusphere-2026-2688
Preprint. Discussion started: 11 June 2026

We note that the correlations reported in this work, while robust across multiple satellite datasets, establish statistical associations rather than direct causal relationships. The proposed bottom-up mechanism and the double-celled anomalous circulation represent observationally based hypotheses whose validation requires dedicated numerical model experiments. Such experiments will be an essential next step to elucidate the role of PMCs in mesospheric H_2O transport, to quantify the relative contributions of chemical and dynamical heating, and to establish causality within the coupled system.

Data Availability. The MLS Level 2, version 5 data are available for download from the NASA GES DISC website. Specifically, the MLS water vapor data can be accessed at https://disc.gsfc.nasa.gov/datasets/ML2H2O_005/summary, the ozone data at https://disc.gsfc.nasa.gov/datasets/ML2O3_005/summary, and the temperature data at https://disc.gsfc.nasa.gov/datasets/ML2T_005/summary. The quality document of MLS is available at https://mls.jpl.nasa.gov/data/v5-0_data_quality_document.pdf. The SABER data version 2.07 of temperature, ozone, atomic oxygen, and atomic hydrogen can be download from https://data.gats-inc.com/saber/Version2_0/SABER_atox/.

Author Contributions. Liang Zhang conceived the idea, analyzed the data, and drafted the manuscript. Zhongfang Liu revised the paper.

Competing Interests. The authors declare that they have no conflict of interests.

Acknowledgements. We are especially grateful to the MLS and SABER program for providing us with the long-range and high-quality data.

Financial support. This research has been supported the National Natural Science Foundation of China (42025602 and 41905059).

References

Bailey, S. M., Thurairajah, B., Hervig, M. E., Siskind, D. E., Russell, J. M. and Gordley, L. L. (2021), Trends in the polar summer mesosphere temperature and pressure altitude from satellite observations, *Journal of Atmospheric and Solar-Terrestrial Physics*, *220*, 105650, https://doi.org/10.1016/j.jastp.2021.105650.

Balsley, B. B. and Riddle, A. C. (1984), Monthly Mean Values of the Mesospheric Wind Field over Poker Flat, Alaska, *Journal of Atmospheric Sciences*, *41*(15), 2368-2380, https://doi.org/10.1175/1520-0469(1984)041<2368:MMVOTM>2.0.CO;2.

Becker, E. (2012), Dynamical Control of the Middle Atmosphere, *Space Science Reviews*, *168*(1), 283-314, https://doi.org/10.1007/s11214-011-9841-5.

https://doi.org/10.5194/egusphere-2026-2688
Preprint. Discussion started: 11 June 2026

Beig, G. (2011a), Long-term trends in the temperature of the mesosphere/lower thermosphere region: 1. Anthropogenic influences, *Journal of Geophysical Research: Space Physics*, *116*(A2), https://doi.org/10.1029/2011JA016646.

Beig, G. (2011b), Long-term trends in the temperature of the mesosphere/lower thermosphere region: 2. Solar response, *Journal of Geophysical Research: Space Physics*, *116*(A2), https://doi.org/10.1029/2011JA016766.

Berger, U. and von Zahn, U. (2002), Icy particles in the summer mesopause region: Three-dimensional modeling of their environment and two-dimensional modeling of their transport, *Journal of Geophysical Research: Space Physics*, *107*(A11), SIA 10-1-SIA 10-32, https://doi.org/10.1029/2001JA000316.

Das, U. (2021), Spatial variability in long-term temperature trends in the middle atmosphere from SABER/TIMED observations, *Advances in Space Research*, *68*(7), 2890-2903, https://doi.org/10.1016/j.asr.2021.05.014.

Eswaraiah, S., Venkat Ratnam, M., Krishna Murthy, B. V. and Vijaya Bhaskara Rao, S. (2011), Low-latitude mesospheric vertical winds observed using VHF radar, *Journal of Geophysical Research: Atmospheres*, *116*(D22), https://doi.org/10.1029/2011JD016385.

García-Comas, M., Funke, B., Gardini, A., López-Puertas, M., Jurado-Navarro, A., von Clarmann, T., Stiller, G., Kiefer, M., Boone, C. D., Leblanc, T., Marshall, B. T., Schwartz, M. J. and Sheese, P. E. (2014), MIPAS temperature from the stratosphere to the lower thermosphere: Comparison of vM21 with ACE-FTS, MLS, OSIRIS, SABER, SOFIE and lidar measurements, *Atmos. Meas. Tech.*, *7*(11), 3633-3651, https://doi.org/10.5194/amt-7-3633-2014.

Garcia, R. R. and Solomon, S. (1985), The effect of breaking gravity waves on the dynamics and chemical composition of the mesosphere and lower thermosphere, *Journal of Geophysical Research: Atmospheres*, *90*(D2), 3850-3868, https://doi.org/10.1029/JD090iD02p03850.

Gattinger, R. L., Kyrölä, E., Boone, C. D., Evans, W. F. J., Walker, K. A., McDade, I. C., Bernath, P. F. and Llewellyn, E. J. (2013), The roles of vertical advection and eddy diffusion in the equatorial mesospheric semi-annual oscillation (MSAO), *Atmospheric Chemistry and Physics*, *13*(15), 7813-7824, https://doi.org/10.5194/acp-13-7813-2013.

Grygalashvyly, M., Ward, W., Stephan, C. C. and Hartogh, P. (2025), Chemical Heating as a Feedback Mechanism in the Mesopause Region, *Geophysical Research Letters*, *52*(20), e2025GL118709, https://doi.org/10.1029/2025GL118709.

Gu, S., Zhao, H., Wei, Y., Wang, D. and Dou, X. (2022), Atomic Oxygen SAO, AO and QBO in the Mesosphere and Lower Thermosphere Based on Measurements from SABER on TIMED during 2002–2019, in *Atmosphere*, edited, p. 517, https://doi.org/10.3390/atmos13040517.

Gudadze, N., Stober, G. and Chau, J. L. (2019), Can VHF radars at polar latitudes measure mean vertical winds in the presence of PMSE?, *Atmos. Chem. Phys.*, *19*(7), 4485-4497, https://doi.org/10.5194/acp-19-4485-2019.

Guiu, J. M., Bakker, J. M., Bernhardt, T. M., Plane, J. M. C., Bromley, S. T. and Lang, S. M. (2025), Oxygen-rich anionic metal silicate clusters as nucleation seeds for noctilucent clouds, *npj Climate and Atmospheric Science*, *8*(1), 153, https://doi.org/10.1038/s41612-025-01019-7.

Gumbel, J. and Megner, L. (2009), Charged meteoric smoke as ice nuclei in the mesosphere: Part 1—A review of basic concepts, *Journal of Atmospheric and Solar-Terrestrial Physics*, *71*(12), 1225-1235, https://doi.org/10.1016/j.jastp.2009.04.012.

Hays, P. B. and Roble, R. G. (1973), Observation of mesospheric ozone at low latitudes, *Planetary and Space Science*, *21*(2), 273-279, https://doi.org/10.1016/0032-0633(73)90011-1.

Hervig, M., McHugh, M. and Summers, M. E. (2003), Water vapor enhancement in the polar summer mesosphere and its relationship to polar mesospheric clouds, *Geophysical Research Letters*, *30*(20), https://doi.org/10.1029/2003GL018089.

https://doi.org/10.5194/egusphere-2026-2688
Preprint. Discussion started: 11 June 2026

Hervig, M. E., Siskind, D. E., Bailey, S. M. and Russell III, J. M. (2015), The influence of PMCs on water vapor and drivers behind PMC variability from SOFIE observations, *Journal of Atmospheric and Solar-Terrestrial Physics*, *132*, 124-134, https://doi.org/10.1016/j.jastp.2015.07.010.

Holton, J. R. (1983), The Influence of Gravity Wave Breaking on the General Circulation of the Middle Atmosphere, *Journal of Atmospheric Sciences*, *40*(10), 2497-2507, https://doi.org/10.1175/1520-0469(1983)040<2497:TIOGWB>2.0.CO;2.

Hultgren, K. and Gumbel, J. (2014), Tomographic and spectral views on the lifecycle of polar mesospheric clouds from Odin/OSIRIS, *Journal of Geophysical Research: Atmospheres*, *119*(24), 14,129-14,143, https://doi.org/10.1002/2014JD022435.

Jiang, Y. B., Froidevaux, L., Lambert, A., Livesey, N. J., Read, W. G., Waters, J. W., Bojkov, B., Leblanc, T., McDermid, I. S., Godin-Beekmann, S., Filipiak, M. J., Harwood, R. S., Fuller, R. A., Daffer, W. H., Drouin, B. J., Cofield, R. E., Cuddy, D. T., Jarnot, R. F., Knosp, B. W., Perun, V. S., Schwartz, M. J., Snyder, W. V., Stek, P. C., Thurstans, R. P., Wagner, P. A., Allaart, M., Andersen, S. B., Bodeker, G., Calpini, B., Claude, H., Coetzee, G., Davies, J., De Backer, H., Dier, H., Fujiwara, M., Johnson, B., Kelder, H., Leme, N. P., König-Langlo, G., Kyro, E., Laneve, G., Fook, L. S., Merrill, J., Morris, G., Newchurch, M., Oltmans, S., Parrondos, M. C., Posny, F., Schmidlin, F., Skrivankova, P., Stubi, R., Tarasick, D., Thompson, A., Thouret, V., Viatte, P., Vömel, H., von Der Gathen, P., Yela, M. and Zablocki, G. (2007), Validation of Aura Microwave Limb Sounder Ozone by ozonesonde and lidar measurements, *Journal of Geophysical Research: Atmospheres*, *112*(D24), https://doi.org/10.1029/2007JD008776.

Karlsson, B. and Kuilman, M. (2018), On How the Middle Atmospheric Residual Circulation Responds to the Solar Cycle Close to the Solstices, *Journal of Climate*, *31*(1), 401-421, https://doi.org/10.1175/JCLI-D-17-0202.1.

Kaufmann, M., Gusev, O. A., Grossmann, K. U., Martín-Torres, F. J., Marsh, D. R. and Kutepov, A. A. (2003), Satellite observations of daytime and nighttime ozone in the mesosphere and lower thermosphere, *Journal of Geophysical Research: Atmospheres*, *108*(D9), https://doi.org/10.1029/2002JD002800.

Kishore Kumar, G., Kishore Kumar, K., Singer, W., Zülicke, C., Gurubaran, S., Baumgarten, G., Ramkumar, G., Sathishkumar, S. and Rapp, M. (2014), Mesosphere and lower thermosphere zonal wind variations over low latitudes: Relation to local stratospheric zonal winds and global circulation anomalies, *Journal of Geophysical Research: Atmospheres*, *119*(10), 5913-5927, https://doi.org/10.1002/2014JD021610.

Kulikov, M. Y., Belikovich, M. V., Grygalashvyly, M., Sonnemann, G. R., Ermakova, T. S., Nechaev, A. A. and Feigin, A. M. (2018a), Nighttime Ozone Chemical Equilibrium in the Mesopause Region, *Journal of Geophysical Research: Atmospheres*, *123*(6), 3228-3242, https://doi.org/10.1002/2017JD026717.

Kulikov, M. Y., Nechaev, A. A., Belikovich, M. V., Ermakova, T. S. and Feigin, A. M. (2018b), Technical note: Evaluation of the simultaneous measurements of mesospheric OH, HO2, and O3 under a photochemical equilibrium assumption – a statistical approach, *Atmos. Chem. Phys.*, *18*(10), 7453-7471, https://doi.org/10.5194/acp-18-7453-2018.

Kulikov, M. Y., Nechaev, A. A., Belikovich, M. V., Vorobeva, E. V., Grygalashvyly, M., Sonnemann, G. R. and Feigin, A. M. (2019), Boundary of Nighttime Ozone Chemical Equilibrium in the Mesopause Region From SABER Data: Implications for Derivation of Atomic Oxygen and Atomic Hydrogen, *Geophysical Research Letters*, *46*(2), 997-1004, https://doi.org/10.1029/2018GL080364.

Laštovička, J. (2017), A review of recent progress in trends in the upper atmosphere, *Journal of Atmospheric and Solar-Terrestrial Physics*, *163*, 2-13, https://doi.org/10.1016/j.jastp.2017.03.009.

Lee, J. N. and Wu, D. L. (2020), Solar Cycle Modulation of Nighttime Ozone Near the Mesopause as Observed by MLS, *Earth and Space Science*, *7*(4), e2019EA001063, https://doi.org/10.1029/2019EA001063.

https://doi.org/10.5194/egusphere-2026-2688
Preprint. Discussion started: 11 June 2026

Lindzen, R. S. (1981), Turbulence and stress owing to gravity wave and tidal breakdown, *Journal of Geophysical Research*, *86*(C10), 9707-9714, https://doi.org/10.1029/JC086iC10p09707.

Liu, X., Xu, J., Yue, J., Liu, Y. and Andrioli, V. F. (2024), Trends in the high-latitude mesosphere temperature and mesopause revealed by SABER, *Atmospheric Chemistry and Physics*, *24*(17), 10143-10157, https://doi.org/10.5194/acp-24-10143-2024.

Lossow, S., Urban, J., Gumbel, J., Eriksson, P. and Murtagh, D. (2008), Observations of the mesospheric semi-annual oscillation (MSAO) in water vapour by Odin/SMR, *Atmospheric Chemistry and Physics*, *8*(21), 6527-6540, https://doi.org/10.5194/acp-8-6527-2008.

Lübken, F.-J., Berger, U. and Baumgarten, G. (2013), Temperature trends in the midlatitude summer mesosphere, *Journal of Geophysical Research: Atmospheres*, *118*(24), 13,347-13,360, https://doi.org/10.1002/2013JD020576.

Marsh, D., Smith, A. and Noble, E. (2003), Mesospheric ozone response to changes in water vapor, *Journal of Geophysical Research: Atmospheres*, *108*(D3), https://doi.org/10.1029/2002JD002705.

Megner, L. and Gumbel, J. (2009), Charged meteoric particles as ice nuclei in the mesosphere: Part 2: A feasibility study, *Journal of Atmospheric and Solar-Terrestrial Physics*, *71*(12), 1236-1244, https://doi.org/10.1016/j.jastp.2009.05.002.

Mlynczak, M. G., Hunt, L. A., Garcia, R., Lopez-Puertas, M., Mertens, C. J., Nowak, N. and Marshall, B. T. (2024), Energy Conservation in the Cooling and Contracting Upper Mesosphere and Lower Thermosphere, *Geophysical Research Letters*, *51*(14), e2024GL109757, https://doi.org/10.1029/2024GL109757.

Mlynczak, M. G., Hunt, L. A., Garcia, R. R., Harvey, V. L., Marshall, B. T., Yue, J., Mertens, C. J. and Russell III, J. M. (2022), Cooling and Contraction of the Mesosphere and Lower Thermosphere From 2002 to 2021, *Journal of Geophysical Research: Atmospheres*, *127*(22), e2022JD036767, https://doi.org/10.1029/2022JD036767.

Mlynczak, M. G., Hunt, L. A., Marshall, B. T., Mertens, C. J., Marsh, D. R., Smith, A. K., Russell, J. M., Siskind, D. E. and Gordley, L. L. (2014), Atomic hydrogen in the mesopause region derived from SABER: Algorithm theoretical basis, measurement uncertainty, and results, *Journal of Geophysical Research: Atmospheres*, *119*(6), 3516-3526, https://doi.org/10.1002/2013JD021263.

Mlynczak, M. G., Hunt, L. A., Mast, J. C., Thomas Marshall, B., Russell Iii, J. M., Smith, A. K., Siskind, D. E., Yee, J.-H., Mertens, C. J., Javier Martin-Torres, F., Earl Thompson, R., Drob, D. P. and Gordley, L. L. (2013), Atomic oxygen in the mesosphere and lower thermosphere derived from SABER: Algorithm theoretical basis and measurement uncertainty, *Journal of Geophysical Research: Atmospheres*, *118*(11), 5724-5735, https://doi.org/10.1002/jgrd.50401.

Mlynczak, M. G., Hunt, L. A., Russell Iii, J. M. and Marshall, B. T. (2018), Updated SABER Night Atomic Oxygen and Implications for SABER Ozone and Atomic Hydrogen, *Geophysical Research Letters*, *45*(11), 5735-5741, https://doi.org/10.1029/2018GL077377.

Mlynczak, M. G. and Solomon, S. (1993), A detailed evaluation of the heating efficiency in the middle atmosphere, *Journal of Geophysical Research: Atmospheres*, *98*(D6), 10517-10541, https://doi.org/10.1029/93JD00315.

Murray, B. J. and Plane, J. M. C. (2005), Modelling the impact of noctilucent cloud formation on atomic oxygen and other minor constituents of the summer mesosphere, *Atmos. Chem. Phys.*, *5*(4), 1027-1038, https://doi.org/10.5194/acp-5-1027-2005.

Plane, J. M. C., Gumbel, J., Kalogerakis, K. S., Marsh, D. R. and von Savigny, C. (2023), Opinion: Recent developments and future directions in studying the mesosphere and lower thermosphere, *Atmospheric Chemistry and Physics*, *23*(20), 13255-13282, https://doi.org/10.5194/acp-23-13255-2023.

https://doi.org/10.5194/egusphere-2026-2688
Preprint. Discussion started: 11 June 2026

Ramesh, K., Mitchell, N. J., Hindley, N. P. and Moffat-Griffin, T. (2024), Long-Term Variability and Tendencies in Mesosphere and Lower Thermosphere Winds From Meteor Radar Observations Over Esrange (67.9°N, 21.1°E), *Journal of Geophysical Research: Atmospheres*, *129*(7), e2023JD040404, https://doi.org/10.1029/2023JD040404.

Ramesh, K., Sridharan, S. and Vijaya Bhaskara Rao, S. (2015), Influence of solar cycle and chemistry on tropical (10°N–15°N) mesopause variabilities, *Journal of Geophysical Research: Space Physics*, *120*(5), 4038-4051, https://doi.org/10.1002/2014JA020930.

Rapp, M. and Thomas, G. E. (2006), Modeling the microphysics of mesospheric ice particles: Assessment of current capabilities and basic sensitivities, *Journal of Atmospheric and Solar-Terrestrial Physics*, *68*(7), 715-744, https://doi.org/10.1016/j.jastp.2005.10.015.

Remsberg, E. E., Marshall, B. T., Garcia-Comas, M., Krueger, D., Lingenfelser, G. S., Martin-Torres, J., Mlynczak, M. G., Russell Iii, J. M., Smith, A. K., Zhao, Y., Brown, C., Gordley, L. L., Lopez-Gonzalez, M. J., Lopez-Puertas, M., She, C. Y., Taylor, M. J. and Thompson, R. E. (2008), Assessment of the quality of the Version 1.07 temperature-versus-pressure profiles of the middle atmosphere from TIMED/SABER, *Journal of Geophysical Research: Atmospheres*, *113*(D17), https://doi.org/10.1029/2008JD010013.

Rong, P. P., Russell Iii, J. M., Mlynczak, M. G., Remsberg, E. E., Marshall, B. T., Gordley, L. L. and López-Puertas, M. (2009), Validation of Thermosphere Ionosphere Mesosphere Energetics and Dynamics/Sounding of the Atmosphere using Broadband Emission Radiometry (TIMED/SABER) v1.07 ozone at 9.6 μm in altitude range 15–70 km, *Journal of Geophysical Research: Atmospheres*, *114*(D4), https://doi.org/10.1029/2008JD010073.

Russell, J., Mlynczak, M., Gordley, L., Tansock, J. and Esplin, R. (1999), Overview of the SABER experiment and preliminary calibration results, *SPIE Proceedings*, *3756*(20), 277-288, https://doi.org/10.1117/12.366382.

Siskind, D. E., Marsh, D. R., Mlynczak, M. G., Martin-Torres, F. J. and Russell Iii, J. M. (2008), Decreases in atomic hydrogen over the summer pole: Evidence for dehydration from polar mesospheric clouds?, *Geophysical Research Letters*, *35*(13), https://doi.org/10.1029/2008GL033742.

Siskind, D. E., Merkel, A. W., Marsh, D. R., Randall, C. E., Hervig, M. E., Mlynczak, M. G. and Russell Iii, J. M. (2018), Understanding the Effects of Polar Mesospheric Clouds on the Environment of the Upper Mesosphere and Lower Thermosphere, *Journal of Geophysical Research: Atmospheres*, *123*(20), 11,705-11,719, https://doi.org/10.1029/2018JD028830.

Smith, A. K. (2012), Global Dynamics of the MLT, *Surveys in Geophysics*, *33*(6), 1177-1230, https://doi.org/10.1007/s10712-012-9196-9.

Smith, A. K., Espy, P. J., López-Puertas, M. and Tweedy, O. V. (2018), Spatial and Temporal Structure of the Tertiary Ozone Maximum in the Polar Winter Mesosphere, *Journal of Geophysical Research: Atmospheres*, *123*(8), 4373-4389, https://doi.org/10.1029/2017JD028030.

Smith, A. K., Harvey, V. L., Mlynczak, M. G., Funke, B., García-Comas, M., Hervig, M., Kaufmann, M., Kyrölä, E., López-Puertas, M., McDade, I., Randall, C. E., Russell Iii, J. M., Sheese, P. E., Shiotani, M., Skinner, W. R., Suzuki, M. and Walker, K. A. (2013), Satellite observations of ozone in the upper mesosphere, *Journal of Geophysical Research: Atmospheres*, *118*(11), 5803-5821, https://doi.org/10.1002/jgrd.50445.

Smith, A. K. and Marsh, D. R. (2005), Processes that account for the ozone maximum at the mesopause, *Journal of Geophysical Research: Atmospheres*, *110*(D23), https://doi.org/10.1029/2005JD006298.

Stober, G., Liu, A., Kozlovsky, A., Qiao, Z., Kuchar, A., Jacobi, C., Meek, C., Janches, D., Liu, G., Tsutsumi, M., Gulbrandsen, N., Nozawa, S., Lester, M., Belova, E., Kero, J. and Mitchell, N. (2022), Meteor radar vertical wind observation biases and mathematical debiasing strategies including the 3DVAR+DIV algorithm, *Atmos. Meas. Tech.*, *15*(19), 5769-5792, https://doi.org/10.5194/amt-15-5769-2022.

https://doi.org/10.5194/egusphere-2026-2688
Preprint. Discussion started: 11 June 2026

Summers, M. E., Conway, R. R., Englert, C. R., Siskind, D. E., Stevens, M. H., Russell Iii, J. M., Gordley, L. L. and McHugh, M. J. (2001), Discovery of a water vapor layer in the Arctic summer mesosphere: Implications for polar mesospheric clouds, *Geophysical Research Letters*, *28*(18), 3601-3604, https://doi.org/10.1029/2001GL013217.

Urco, J. M., Feraco, F., Chau, J. L. and Marino, R. (2024), Augmented Four-Dimensional Mesosphere and Lower Thermosphere Wind Field Reconstruction via the Physics-Informed Machine Learning Approach HYPER, *Journal of Geophysical Research: Machine Learning and Computation*, *1*(3), e2024JH000162, https://doi.org/10.1029/2024JH000162.

Vellalassery, A., Baumgarten, G., Grygalashvyly, M., Lübken, F.-J. and Udayakumar, G. (2026), Influence of atmospheric vertical wind and turbulence on noctilucent clouds, *Frontiers in Astronomy and Space Sciences*, *Volume 13 - 2026*, https://doi.org/10.3389/fspas.2026.1721062.

von Zahn, U. and Berger, U. (2003), Persistent ice cloud in the midsummer upper mesosphere at high latitudes: Three-dimensional modeling and cloud interactions with ambient water vapor, *Journal of Geophysical Research: Atmospheres*, *108*(D8), https://doi.org/10.1029/2002JD002409.

Wu, X., Zhu, Y., Smith, A. K., Kaufmann, M., Jiang, G., Liu, S. and Xu, J. (2026), A new data set of nighttime chemical heating rates in the upper mesosphere and lower thermosphere derived from SCIAMACHY OH (9–6) emissions and SABER profiles, *Atmos. Chem. Phys.*, *26*(7), 4669-4683, https://doi.org/10.5194/acp-26-4669-2026.

Xu, J., Smith, A. K., Yuan, W., Liu, H. L., Wu, Q., Mlynczak, M. G. and Russell Iii, J. M. (2007), Global structure and long-term variations of zonal mean temperature observed by TIMED/SABER, *Journal of Geophysical Research: Atmospheres*, *112*(D24), https://doi.org/10.1029/2007JD008546.

Yuan, T., She, C. Y., Oberheide, J. and Krueger, D. A. (2014), Vertical tidal wind climatology from full-diurnal-cycle temperature and Na density lidar observations at Ft. Collins, CO (41°N, 105°W), *Journal of Geophysical Research: Atmospheres*, *119*(8), 4600-4615, https://doi.org/10.1002/2013JD020338.

Zeng, J., Stober, G., Yi, W., Xue, X., Zhong, W., Reid, I., Adami, C., Ning, B., Li, G. and Dou, X. (2024), Mesosphere/Lower Thermosphere 3-Dimensional Spatially Resolved Winds Observed by Chinese Multistatic Meteor Radar Network Using the Newly Developed VVP Method, *Journal of Geophysical Research: Atmospheres*, *129*(11), e2023JD040642, https://doi.org/10.1029/2023JD040642.

Zhang, L., Liu, Z. and Tinsley, B. (2025a), Altitude-dependent formation of polar mesospheric clouds: charged nucleation and in situ ice growth on zonal and daily scales, *Atmos. Chem. Phys.*, *25*(19), 12701-12719, https://doi.org/10.5194/acp-25-12701-2025.

Zhang, L., Liu, Z. and Tinsley, B. (2025b), Height-Latitude Patterns of Interannual Climate Variability in the Upper Mesosphere and Lower Thermosphere During Spring and Autumn Months, *Geophysical Research Letters*, *52*(13), e2025GL116281, https://doi.org/10.1029/2025GL116281.

Zhang, L., Liu, Z. and Tinsley, B. (2025c), Interhemispheric Anti-Phase Variability in Mesospheric Climate Driven by Summer Polar Upwelling During Solstice Months, *Atmos. Chem. Phys.*, *25*(20), 13141-13159, https://doi.org/10.5194/acp-25-13141-2025.

Zhang, L., Tinsley, B. and Zhou, L. (2022), Responses of CIPS/AIM noctilucent clouds to the interplanetary magnetic field, *Atmospheric Chemistry and Physics*, *22*(20), 13355-13370, https://doi.org/10.5194/acp-22-13355-2022.

Zhao, X. R., Sheng, Z., Shi, H. Q., Weng, L. B. and Liao, Q. X. (2020), Long-Term Trends and Solar Responses of the Mesopause Temperatures Observed by SABER During the 2002–2019 Period, *Journal of Geophysical Research: Atmospheres*, *125*(11), e2020JD032418, https://doi.org/10.1029/2020JD032418.

Zhu, Y. and Kaufmann, M. (2018), Atomic Oxygen Abundance Retrieved From SCIAMACHY Hydroxyl Nightglow Measurements, *Geophysical Research Letters*, *45*(17), 9314-9322, https://doi.org/10.1029/2018GL079259.